OXFORD

Cerebral Cortex, February 2017;27: 1037–1059

doi:10.1093/cercor/bhv288
Advance Access Publication Date: 7 December 2015
Original Article

ORIGINAL ARTICLE

Is There a Nonadditive Interaction Between Spontaneous and Evoked Activity? Phase-Dependence and Its Relation to the Temporal Structure of Scale-Free Brain Activity

Zirui Huang[1], Jianfeng Zhang[2,3], André Longtin[4], Grégory Dumont[1,4], Niall W. Duncan[1,2,5], Johanna Pokorny[6], Pengmin Qin[1,5], Rui Dai[2,3,7], Francesca Ferri[1], Xuchu Weng[2,3] and Georg Northoff[1,2,3,5]

[1]Institute of Mental Health Research, University of Ottawa, Ottawa, ON K1Z 7K4, Canada, [2]Center for Cognition and Brain Disorders, Hangzhou Normal University, Hangzhou 311121, PR China, [3]Zhejiang Key Laboratory for Research in Assessment of Cognitive Impairments, Hangzhou Normal University, Hangzhou 310015, PR China, [4]Department of Physics, University of Ottawa, Ottawa, ON K1N 6N5, Canada, [5]Brain and Consciousness Research Center, Taipei Medical University-Shuang Ho Hospital, New Taipei City 23561, Taiwan, [6]Department of Anthropology, University of Toronto, Toronto, ON M5S 2S2, Canada and [7]School of Life Science, South China Normal University, Guangzhou 510613, PR China

Address correspondence to Zirui Huang, Mind, Brain Imaging and Neuroethics, University of Ottawa Institute of Mental Health Research, Room 6440, 1145 Carling Ave, Ottawa, Ontario, K1Z 7K4, Canada. Email: dr.zirui.huang@gmail.com

Abstract

The aim of our study was to use functional magnetic resonance imaging to investigate how spontaneous activity interacts with evoked activity, as well as how the temporal structure of spontaneous activity, that is, long-range temporal correlations, relate to this interaction. Using an extremely sparse event-related design (intertrial intervals: 52–60 s), a novel blood oxygen level-dependent signal correction approach (accounting for spontaneous fluctuations using pseudotrials) and phase analysis, we provided direct evidence for a nonadditive interaction between spontaneous and evoked activity. We demonstrated the discrepancy between the present and previous observations on why a linear superposition between spontaneous and evoked activity can be seen by using co-occurring signals from homologous brain regions. Importantly, we further demonstrated that the nonadditive interaction can be characterized by phase-dependent effects of spontaneous activity, which is closely related to the degree of long-range temporal correlations in spontaneous activity as indexed by both power-law exponent and phase–amplitude coupling. Our findings not only contribute to the understanding of spontaneous brain activity and its scale-free properties, but also bear important implications for our understanding of neural activity in general.

Key words: fMRI, infraslow frequency, scale-free property, spontaneous activity, trial-to-trial variability

Introduction

Imagine you are surfing on a rough ocean; you have to adjust your surfboard according to the constant motion of the waves. Our spontaneous brain activity is similar to this rough ocean, fluctuating all the time, and further, we can think of the surfboard as incoming evoked activity. In this surfing scenario, your surfboard and you are interacting dynamically with the ocean rather than merely "standing" on it. Similarly in the fluctuating brain, it seems intuitive that evoked activity might also interact dynamically with the ongoing spontaneous activity, rather than simply being added or "standing" on it. However, it remains unclear whether spontaneous and evoked activity are linearly superimposed (Arieli et al. 1996; Azouz and Gray 1999; Fox et al. 2006; Becker et al. 2011), the view which predominates in the neuroscientific literature, or interact in a nonadditive way as suggested in several studies (Hesselmann, Kell and Eger et al. 2008; Hesselmann, Kell and Kleinschmidt 2008; Sadaghiani et al. 2009, 2010; Northoff et al. 2010; He 2013). Recently, an elegant functional magnetic resonance imaging (fMRI) study has shed doubt on the linear assumption and proposed a nonadditive, namely, negative interaction between spontaneous and evoked activity (He 2013). That is, stimuli presented at a lower magnitude of the preceding spontaneous activity fluctuations will produce a stronger response than stimuli presented at a higher magnitude. However, more direct evidence for such nonadditive interaction as well as a comprehensive demonstration of the apparent discrepancies reported in the literature (e.g., Fox et al. 2006; He 2013) has to be achieved.

Furthermore, focusing on the influence of the magnitude of the prestimulus spontaneous activity on evoked activity may not provide the complete picture, as it overlooks the fact that activity of the same magnitude can be at different points on the activity's wave progression (i.e., on the up- or down-stroke); the wave phase of the prestimulus spontaneous activity might have an influence on the evoked activity. To take this factor into account, one needs to study the exact phase of the spontaneous activity, and not just its magnitude (Nir et al. 2007; Yang et al. 2012), although this is often neglected in fMRI studies (Laird et al. 2002; Saad et al. 2003). By doing so, it would be possible to ascertain if a particular point in the phase cycle of spontaneous activity has an effect on the evoked response. This approach, however, has not yet been attempted, and the question as to whether different points in the phase cycle of infraslow spontaneous fluctuations (<0.5 Hz), measured by fMRI (He and Raichle 2009), confer different levels of temporal excitability for incoming stimuli remains unanswered.

To further understand the interaction between spontaneous and evoked brain activity, one may also consider how the regularities, or temporal structure, of spontaneous activity in the resting-state are related to this interaction. Interestingly, the temporal structure of spontaneous brain activity, as well as many other natural phenomena, can be characterized by scale-free dynamics, or long-range temporal correlations (LRTCs) (Linkenkaer-Hansen et al. 2001; Manning et al. 2009; Miller et al. 2009; Chialvo 2010; He et al. 2010; Palva et al. 2013). Most importantly, recent fMRI studies show that infraslow spontaneous fluctuations observed in the resting-state conform to a power-law distribution and hence show LRTCs (He et al. 2010; He 2011, 2014). Higher LRTCs, with a larger power-law exponent, are related to a higher time-lagged autocorrelation, indicating that the past pattern of a system has a stronger influence on its future dynamics (Linkenkaer-Hansen et al. 2001). Furthermore, the LRTCs can be characterized by nested frequencies with phase–amplitude coupling (PAC), where the phase of lower frequencies modulates the amplitude of higher ones (Vanhatalo et al. 2004; Canolty et al. 2006; Lakatos et al. 2008; Monto et al. 2008; Tort et al. 2008; He et al. 2010). However, the functional significance of LRTCs (e.g., power-law distribution and phase–amplitude coupling) in spontaneous activity and their possible relationship to the interaction between spontaneous and evoked activity require further study.

The aim of our study was to use fMRI to investigate how spontaneous brain activity interacts with evoked activity, and to ascertain how the temporal structure of spontaneous activity in the resting-state relates to this interaction. More specifically, we organized our questions into 4 lines of investigation: 1) to provide direct evidence for a nonadditive interaction between spontaneous and evoked activity, 2) to investigate the discrepancies reported in the literature in terms of linear superposition (e.g., Fox et al. 2006) and nonadditive interaction (e.g., He 2013); 3) to examine the possible underlying mechanism by considering if the nonadditive interaction can be characterized by the phase of oscillations of spontaneous activity (more specifically, a phase-dependent effect); 4) to understand the neural context of this mechanism by linking phase-dependence to the power-law distribution and PAC of LRTCs in the resting-state.

To this end, we applied a sparse event-related fMRI design with extremely long intertrial intervals (ITIs, 52–60 s) to make sure that the blood–oxygen level-dependent (BOLD) undershoot is terminated, and to obtain a clean baseline of prestimulus spontaneous activity without potential nonlinearities associated with overlapping hemodynamic responses between preceding and subsequent trials (Fox et al. 2006; Yacoub et al. 2006). We used a novel correction method accounting for spontaneous fluctuations using pseudotrials without the application of a stimulus. We introduced Hilbert phase analysis in fMRI signals which was validated, confirmed, and extended in various ways. We then calculated indices for the nonadditive interaction between spontaneous and task-evoked activity as well as the effect of phase-dependence. Finally, we related these indices to the LRTCs of spontaneous activity in the resting-state (acquired during an independent 6-min task-free fMRI scan before any task), as indexed by both power-law exponent (PLE) and PAC.

Materials and Methods

Subjects

Twenty-five right-handed volunteers (12 female; age 20–29 years) participated in this fMRI study. Subjects were all university students with no history of psychiatric or neurological disorders (confirmed using a standard MRI safety screening questionnaire before scanning). They reported understanding verbal experimental instructions and none reported wearing hearing-aids, thus it was assumed that all participants had normal hearing. Written informed consent was obtained from each subject prior to the experiment. The study was approved by the ethics committee of the Center for Cognition and Brain Disorders (CCBD), Hangzhou Normal University. Two subjects were excluded from the analyses because of anxiety and excessive movement during scanning.

Task with Long ITIs

The current experimental design was developed from our previous study (Huang and Dai et al. 2014). Subjects were instructed to fill out a questionnaire with 360 questions about hobbies, birthdays, places visited, and simple facts. All of the questions

contained 6–12 Chinese syllables. Five-point rating scale (1 denoting easiest, 5 denoting hardest) was used to estimate the difficulty of each question. To minimize task difficulty, questions with a score of 3 or above were considered difficult questions and excluded. One hundred twenty questions from these were then selected randomly (after excluding difficult questions) for each subject. As difficult questions made up a very small proportion across all subjects, there was a sufficient number of questions with a score of <3 for each subject. Half of the questions required a "Yes" response and the other half a "No". Each of the questions was digitally recorded into an audio clip lasting 2 s by the same experimenter, and was presented once during the whole fMRI scan session.

An extremely sparse event-related fMRI design was adopted with 120 trials separated by ITIs ranging unpredictably from 52 to 60 s (2 s steps). The benefit of such long ITIs is that they provided sufficient time to include the evoked positive blood–oxygen level-dependent (BOLD) response, as well as the undershoot (Boynton et al. 1996; Yacoub et al. 2006; Hua et al. 2011), and then return to the ongoing "baseline" level. These also avoided potential nonlinearities associated with overlapping hemodynamic responses between preceding and subsequent trials (Fox et al. 2006). These ITIs also enable us to model spontaneous ongoing activity through pseudotrials without the application of a stimulus (from prestimulus 10–1 s, see below). Six fMRI runs were recorded with this paradigm. For each run, 20 trials were assigned pseudorandomly. Each trial was presented for 2 s. The participants were instructed to use their right hands to press left/right buttons on a response box to indicate a yes/no answer (left = yes and right = no) as quickly as possible after question presentation. The button response was monitored during the whole experiment to ensure participant cooperation and alertness.

fMRI Data Acquisition

A GE 3T (Discovery MR750) scanner with a standard head coil (8-channel) was used to acquire gradient-echo EPI images of the whole brain (time repetition, 1.0 s; time echo, 25 ms; 21 slices; slice thickness = 6 mm; spacing = 0; field of view = 210 mm; flip angle = 76°; image matrix: 64 × 64). Task-free "resting-state" data were acquired at the beginning of the whole fMRI experiment with 360 frames (6 min). Each run of the task (6 runs in total) had 1184 frames (19 min 44′). High-resolution anatomical images were acquired at the end of the experiment. During each EPI scan, subjects were instructed to relax, stay awake, and keep their eyes closed. Eye-tracking during fMRI was not available, but off-line post-scan recordings ensured that subjects complied with this instruction. Time-locked cardiac and respiratory signals were recorded. All stimuli were programmed using E-Prime (Psychology Software Tools, Pittsburgh, PA) and delivered via an audiovisual stimulus presentation system designed for an MRI environment. The volume of the headphones was adjusted to the comfort level of each subject.

fMRI Data Preprocessing and Definition of Regions of Interest

Preprocessing steps were implemented in AFNI (http://afni.nimh.nih.gov/afni) including: 1) discarding the first 4 frames of each fMRI run; 2) physiological noise correction through removal of time-locked cardiac and respiratory artifacts using RETROICOR (Glover et al. 2000); 3) slice timing correction; 4) rigid body correction/realignment within and across runs. Head motion parameters were estimated and frame-wise realignment was performed using AFNI's *3dvolreg* command. After the estimated motion parameters were visually inspected, subjects with head motion larger than ±2 mm translation or ±2.5° rotation were eliminated (Johnstone et al. 2006); 5) co-registration with high-resolution anatomical images; 6) spatial normalization into Talaraich stereotactic space; 7) resampling to $3 \times 3 \times 3$ mm^3 voxels; 8) regressing out linear and nonlinear drift (equivalent to a high-pass filtering of 0.0067 Hz), head motion and its temporal derivative, and mean time series from the white matter (WM) and cerebrospinal fluid (CSF) to control for non-neural noise (Fox et al. 2005). The WM and CSF masks were eroded by one voxel (Chai et al. 2012) to minimize partial voluming with gray matter; 9) spatial smoothing with a 6 mm full-width at half-maximum isotropic Gaussian kernel; 10) the time-course per voxel of each run was normalized to zero mean and unit variance (z-value), accounting for differences in variance of non-neural origin (e.g., distance from head coil) (He 2011; Stephens et al. 2013).

All the following analyses were based on regions of interest (ROI) analysis. We adopted a well-established node template from a previous study (Power et al. 2011; Cole et al. 2014), containing 264 putative functional areas (10 mm diameter spheres, 32 voxels per sphere) across the whole brain.

Definition of Real Trials, Pseudotrials, Raw-BOLD and Corrected-BOLD

One of the aims of our study was to measure the nonadditive interaction between spontaneous and evoked activity. We did not assume that evoked activity is linearly superimposed on the spontaneous activity as, for instance, in the general linear model (GLM) (Poline and Brett 2012). Because of this, we chose a simple trial-averaging approach (Gonzalez-Castillo et al. 2012). Two questions were first addressed: 1) How long does it take for the evoked hemodynamic response to reach its peak, and how long does it take for the subsequent undershoot to return to baseline level? 2) How can we obtain a relative BOLD signal change in reference to the prestimulus spontaneous activity levels?

For the first question, the time-courses of the BOLD signal for each of the 264 ROIs were extracted and then averaged across subjects and ROIs, yielding a mean response curve from prestimulus 10 s to poststimulus 43 s (Fig. 1A). This 54-s time window was our maximal time range that could apply to all the trials without any overlapping. From the mean response curve, we observed that the evoked response reached its peak at 6 s after stimulus onset (0 s) and returned to an ongoing baseline level at 43 s after stimulus onset. This is consistent with previous studies (Logothetis et al. 2001; Yacoub et al. 2006; Dechent et al. 2011; Hua et al. 2011). Therefore, the long ITIs (52–60 s) in our study provided a relatively "clean" baseline from 10 to 1 s of prestimulus activity.

To address the second question, we applied pseudotrials (onset: prestimulus 10 s) during the task-free period to model approximate spontaneous activity time-courses as the baseline for the recorded activity (raw-BOLD) (Fig. 1A). By subtracting the averaged raw-BOLD time-course of pseudotrials from that of the real-trials, evoked activity (corrected-BOLD) was recovered. This corrected-BOLD signal was calculated at a resolution of 1 s (one value per TR) in a time range starting from prestimulus 0 s (stimulus onset) and ending 9 s poststimulus (10 time points in total). An example region (ROI-177) in the left inferior parietal lobule (LIPL) within the fronto-parietal task control network (Cole et al. 2014) was used to help demonstrate our analysis

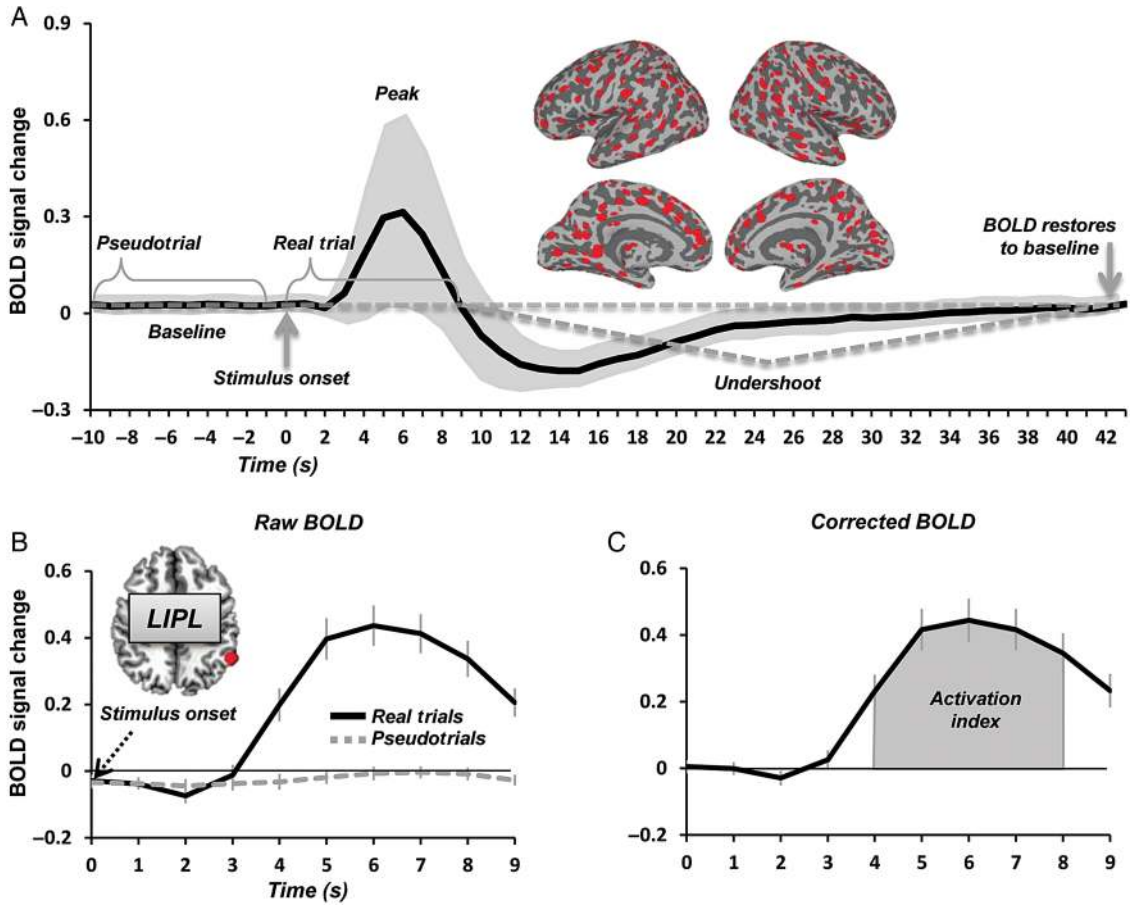

Figure 1. Definition of real trials, pseudotrials, raw-BOLD, corrected-BOLD and activation index. (*A*) Averaged BOLD response across all trials, 264 putative functional areas (Power et al. 2011) and subjects. The time period of task-free activity from prestimulus 10 s (−10 s) to 1 s (−1 s) was used as a relatively "clean" baseline. Pseudotrials (onset: prestimulus 10 s) were applied during this period to model approximate spontaneous activity time-courses as a baseline for the recorded activity (raw-BOLD). Gray shadow zone indicates the ±SD across ROIs. (*B*) Averaged raw-BOLD time-courses (across all trials and subjects) of real and pseudotrials for a representative region (ROI-177 in the LIPL) within the time window from prestimulus 0 s (stimulus-onset) to poststimulus 9 s (same as follows). (*C*) Evoked activity (corrected-BOLD) was obtained by subtracting the raw-BOLD time-course of pseudotrials from that of the real-trials. The "AUC" around the peak of the corrected-BOLD (from poststimulus 4–8 s) was defined as the "activation index". This index was used to detect active regions involved during the fMRI task. Error bars indicate ±SEM.

and results (Fig. 1*B*). Next, we used the "area under the curve" (AUC) around the peak of the corrected-BOLD (from poststimulus 4 s to 8 s) as an "activation index" to quantify the signal changes (Fig. 1*B*). One sample *t*-tests against zero at the group level were used to examine the significance of activation for each region; multiple-comparison errors were controlled using Bonferroni correction across 264 areas, for a corrected threshold of $P < 0.05$ (corresponding to uncorrected $P < 1.89e{-}4$). We restricted our following analysis to those regions showing significant activation and thus which were assumed to be involved in the task (active ROIs) (Fig. 2*A*). Besides these ROIs, we also included several other ROIs (see below for details) to compare our results with a previous study that suggested a linear superposition between spontaneous and evoked activity (Fox et al. 2006).

Trial-To-Trial Variability Analysis

According to the linear superposition model of spontaneous and evoked activity (Arieli et al. 1996; Azouz and Gray 1999; Fox et al. 2006; Becker et al. 2011), the variance of the activities should sum up, a direct consequence of the Law of Total Variance. If this is true, one would expect to find an increase of variability after stimulus onset. However, a recent fMRI study reported a decrease in trial-to-trial variability after stimulus-onset across widespread cortical regions (He 2013). Given the Law of Total Variance, this finding suggests that evoked and spontaneous brain activities are not independent but rather interact nonadditively, and further, since the variability decreases, the interaction can be characterized as a negative interaction (He 2013). Using a similar approach, we also examined the standard deviation (SD) at each time point across trials within the time window (0–9 s as above). The SD time-course of each ROI of each subject was normalized by subtracting and dividing by the SD at stimulus onset (0 s) (He 2013). The AUC (4–8 s) of the normalized SD time-course across trials (real trials only) was defined as the trial-to-trial variability (TTV) index to quantify the gain of TTV changes (Fig. 2*B*). One sample *t*-tests against zero at the group level were used to examine the significance of the TTV index for each region.

Magnitude-Based Analysis

To examine whether the level of evoked activity (corrected-BOLD) depends on whether the stimulus coincides with a high, as opposed to a low, magnitude of the prestimulus activity, all trials for each subject were sorted into 2 equal-sized bins (median split) based on the BOLD magnitude (high and low) at prestimulus

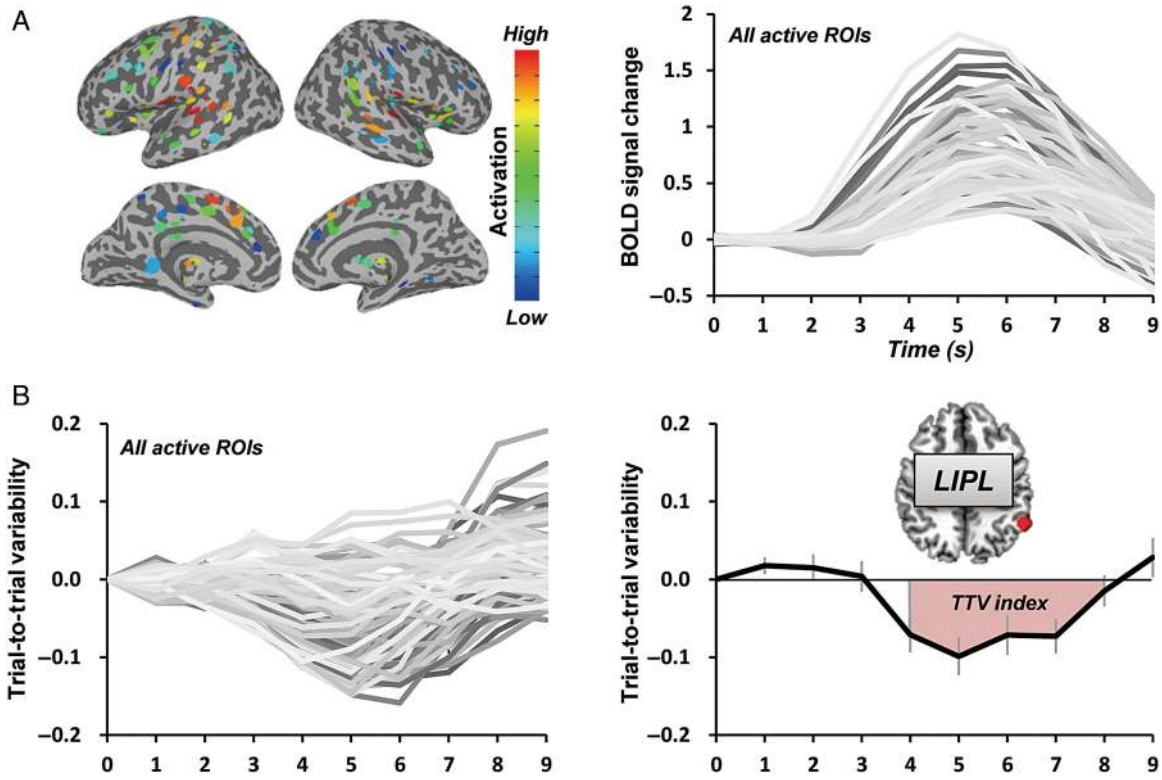

Figure 2. Definition of ROIs, TTV index, and LH index. (*A*) Significant activations were observed in 111 functional areas. These areas were defined as ROIs showing in a surface view of the brain (left), as well as their BOLD time-courses (0–9 s) (right). (*B*) The SD across trials at each time point is shown. For each ROI, the SD time-course (0–9 s) was normalized by subtracting and dividing the SD at prestimulus 0 s, and then averaged across subjects (left). The AUC (4–8 s) of the normalized SD time-course was defined as the TTV index to quantify the gain of TTV changes (LIPL as an example) (right). LIPL, left inferior parietal lobule.

0 s (see Fig. 3A for an illustration; Supplementary Fig. 1 and Supplementary Table 4 for a confirmative analysis using a different trial sorting criterion: third split, contrasting top 33% vs. low 33%). The present analyses were based on comparing trials with prestimulus-high magnitude to trials with prestimulus-low magnitude using median split. The averaged raw-BOLD time-courses for prestimulus-high and prestimulus-low trials were extracted for each active ROI and each subject.

In a next step, we sought to obtain corrected-BOLD for both prestimulus-high and prestimulus-low trials. We applied pseudotrials (as above mentioned) to model approximate spontaneous activity for prestimulus-high and prestimulus-low trials, accounting for the intrinsic or nonstimulus-driven autocorrelations (Arieli et al. 1996; Azouz and Gray 1999; Bullmore et al. 2001; Sylvester et al. 2009; He 2011, 2013). To this end, the same median split approach was performed in the pseudotrials. Subtracting the averaged raw-BOLD of pseudotrials from that of the real-trials, corrected-BOLD was obtained for prestimulus-high and prestimulus-low trials, respectively. Next, similarly to the definition of the activation index, the magnitude-based interaction index, low–high (LH) index, was defined by the AUC (4–8 s) differences of the corrected-BOLD between trials with prestimulus-low and prestimulus-high magnitude (Fig. 3B). One sample *t*-tests against zero at the group level were used to examine the significance of the LH index for each region.

Comparing Our BOLD Signal Correction Approach with a Previous One

We sought to compare our approach with a previously adopted method achieved by using co-occurring signals from homologous brain regions (Fox et al. 2006). Specifically, Fox et al. (2006) used the activity in the homologous brain region as a substitute for the ongoing activity in the activated brain region. For instance, the right somatomotor cortex (RMC) was used as a substitute for ongoing activity in the left somatomotor cortex (LMC) during a right-hand motor task (Fox et al. 2006). We thereby examined 3 pairs of regions, including bilateral inferior parietal lobule (ROI-177 and ROI-194), somatomotor cortex and primary auditory cortex. For the first pair, besides our example region, LIPL (ROI-177), we sought to find its homologous brain region, from which the ongoing activity could be used as a substitute. This region was defined as homologous if it was: 1) not significantly involved in the task; 2) from the same resting-state network; and 3) from the contralateral hemisphere of the brain (Fox et al. 2006). Following these criterions, a region (ROI-194) located in the right inferior parietal lobule (RIPL) comprising the same resting-state network with LIPL (i.e., fronto-parietal task control [Power et al. 2011; Cole et al. 2014]) was identified. Importantly, this region was not significantly involved in the task ($P = 0.313$ for activation index).

For the second pair, bilateral somatomotor cortex, we adopted 10-mm diameter spheres centered on the Talairach coordinates of previously published foci by Fox et al. (2006): LMC [−39, −26, 51] and RMC [38, −26, 48] (see Supplementary Table 1 in Fox et al. 2006). Considering that we used a similar task structure (sparse event-related design with a right-handed button press) and the same regions in the somatomotor cortex, our results could be directly compared with the ones reported by Fox et al. 2006.

As our task also strongly involved auditory processing, we defined the third pair of regions—bilateral primary auditory cortex. Specifically, voxels responding to the stimulus were defined by the contrast of stimuli > baseline at group level using a standard

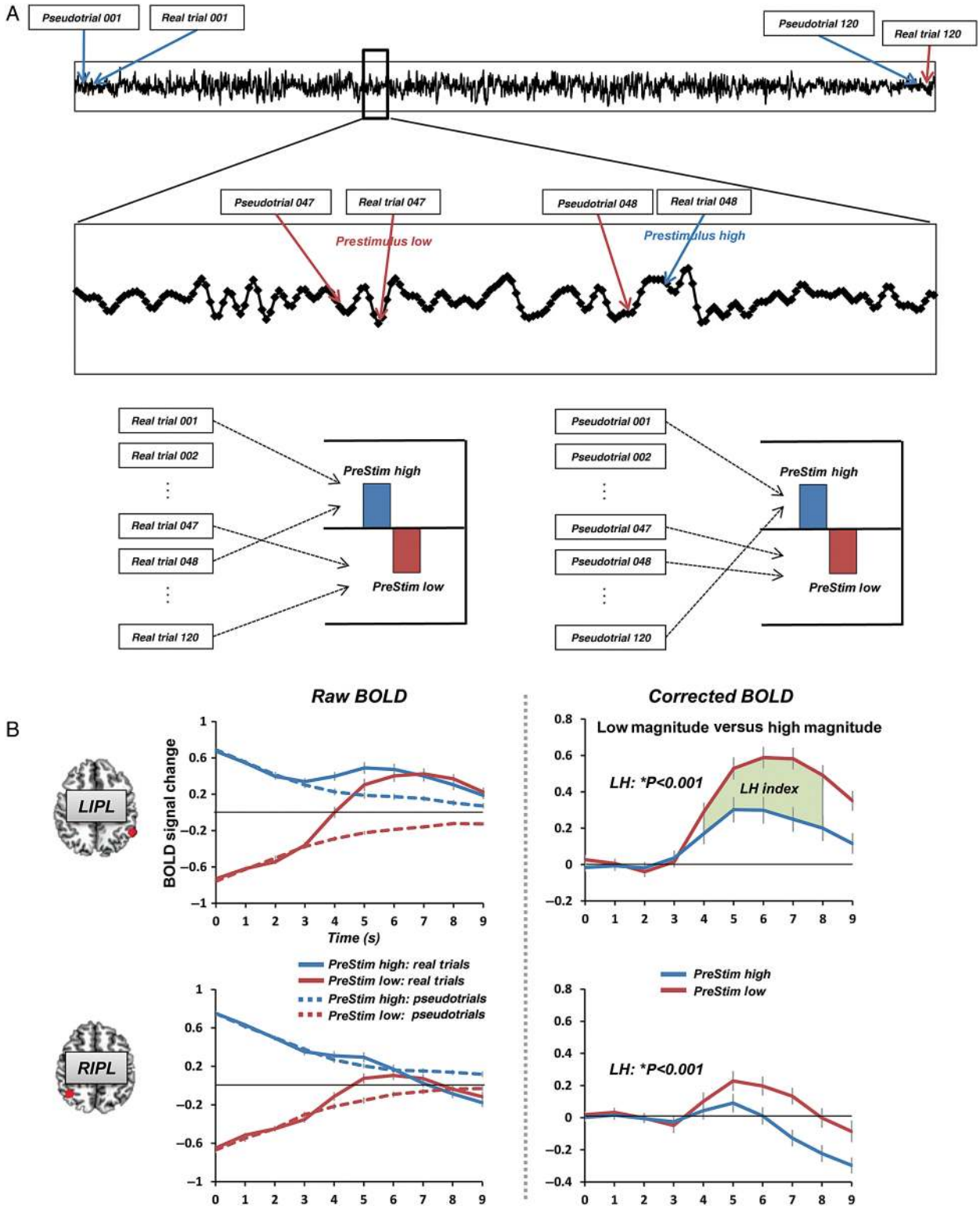

Figure 3. Illustration of magnitude-based analysis and magnitude-based interaction in bilateral inferior parietal lobule (LIPL and RIPL). (*A*) All trials for each subject were sorted into two equal-sized bins (median split) based on the BOLD magnitude (high and low) at prestimulus 0 s. This approach was performed on real and pseudotrials independently. (*B*) Averaged raw-BOLD time-courses of real and pseudotrials for high and low prestimulus BOLD magnitude in the LIPL and RILP (left). Corrected-BOLD time-courses of prestimulus-high and prestimulus-low trials were obtained by subtracting the raw-BOLD of pseudotrials from that of the real-trials (right). The AUC (4–8 s) difference of the corrected-BOLD between trials with prestimulus-low and prestimulus-high magnitude was defined as LH index. Significant interaction was seen in both LIPL and RIPL ($P < 0.001$). Error bars indicate ±SEM.

GLM analysis. The activation map was thresholded at $P < 0.0001$, uncorrected, and cluster extent >100 voxels. This activation map was further masked by anatomically defined masks of BA 41&42 from TT_N27 template in AFNI (Eickhoff et al. 2005) to delineate primary auditory cortices. Finally, the left (LPAC) and right (RPAC) primary auditory cortices were defined by 10-mm diameter spheres centered on the peak voxels of bilateral primary auditory cortex, respectively. The Talairach coordinates of LPAC [−51, −17, 9] and RPAC [51, −15, 6] are in good agreement with previous studies (Morosan et al. 2001; Scott and Johnsrude 2003; Sadaghiani et al. 2009).

The above 3 pairs of regions were then submitted to our magnitude-based analysis. This was followed by submitting LIPL versus RILP and LMC versus RMC to the analysis using co-occurring signals (Fox et al. 2006). As both LPAC and RPAC were significantly activated during the task, they were excluded from the latter approach. We followed the steps reported by Fox et al. (2006) to obtain the corrected-BOLD signal of LIPL and LMC by subtracting the signal of RILP and RMC, respectively. The BOLD signal from RIPL (and RMC) was further scaled by a regression coefficient calculated using the resting-state data and subtracted from the LIPL (and LMC) signal during the task (see Supplementary Methods in Fox et al. 2006 for more details). For each subject, trials were sorted into either a poststimulus-low or poststimulus-high magnitude at the peak time point (6 s after stimulus onset) based on the median magnitude of activity in the RIPL and RMC, respectively. We then computed the AUC (4–8 s) differences of the corrected-BOLD in the LIPL (and LMC) between trials with poststimulus-low and poststimulus-high magnitude. One sample t-tests against zero at the group level were used to examine the significance of the AUC difference.

Validation of Phase Analysis in BOLD Signal

Another aim of this study was to examine whether the nonadditive interaction can be characterized by the phase of the spontaneous BOLD signal. Before doing so, we sought to first validate the phase analysis. We addressed this issue on the basis of traditional functional connectivity (Pearson correlations) analysis of the BOLD signal. We asked whether the whole-brain functional connectivity matrices/pattern (Power et al. 2011; Cole et al. 2014) can be replicated using Hilbert phase and amplitude. In other words, if the phase analysis is producing meaningful information from the fMRI data, then it should produce results that are comparable to those from methods that have previously been assumed to be valid, such as functional connectivity analysis.

We applied the predefined node template (Power et al. 2011; Cole et al. 2014) onto the 6-min resting-state data. The time series of each node was first extracted, and after which the instantaneous phase and amplitude traces were calculated using Hilbert transform (Matlab function "Hilbert") (see Fig. 6A for an illustration). Specifically, this approach treats the BOLD signal $f(t)$ as the real part of a complex signal, called the analytic signal $z(t)$. The imaginary part of $z(t)$ is the Hilbert transform of $f(t)$, and $z(t) = f(t) + iH[f(t)]$. The phase is calculated as the inverse tangent of the ratio of the imaginary and real signals:

$$\theta(t) = \arctan\frac{\mathrm{Im}(z(t))}{\mathrm{Re}(z(t))} = \arctan\frac{H[f(t)]}{f(t)}$$

This method allows calculating instantaneous phase of an ongoing time series even if it is not precisely sinusoidal (Haslinger et al. 2006) which has been used extensively in EEG data analysis (Le Van Quyen et al. 2001; Le Van Quyen and Bragin 2007; Monto et al. 2008; Yang et al. 2012). The phase was "wrapped" so that it was always between $-\pi$ and π, and the instantaneous phase $\theta(t)$ was related to zero crossings and peaks/troughs of the BOLD signal. The amplitude is calculated as the square root of the sum of squares of imaginary and real signals:

$$A(t) = \sqrt{\mathrm{Im}(z(t))^2 + \mathrm{Re}(z(t))^2} = \sqrt{H[f(t)]^2 + [f(t)]^2}$$

In a next step, besides traditional functional connectivity (TFC), we computed 3 other FCs: Kuramoto FC (KFC), Hilbert phase-based FC (PFC), and Hilbert amplitude-based FC (AFC). For the KFC, we measured the averaged phase synchrony across time between a given pair of phase series from 2 nodes. The phase synchrony as a function of time was quantified by the Kuramoto order parameter, $r(t)$, defined by:

$$r(t) = \frac{1}{n}\left|\sum_{j=1}^{n} e^{i\theta_j(t)}\right|,$$

where $n = 2$, as the calculation was performed for each pair of nodes. The KFC was then defined by the mean value of $r(t)$ across time:

$$\mathrm{KFC} = \frac{1}{m}\left|\sum_{t=1}^{m} r(t)\right|,$$

where $m = 356$ is the number of time points in the time series of 6 min resting state (after discarding the first 4 frames). Note that the Kuramoto parameter was originally introduced to measure the degree of synchrony among identical interacting oscillators. Here we used the Kuramoto parameter following Lachaux et al. (1999) for a measure of phase-locking value between brain regions. Afterward, a KFC matrix between all pairs of nodes was obtained for each subject and then averaged across subjects. For the PFC, similarly to the TFC analysis, which uses Pearson correlation, the PFC matrix was computed based on the Hilbert phase series instead of the BOLD signal itself. In a similar way, the AFC matrix was computed based on the Hilbert amplitude series using Pearson correlation.

To this end, we calculated 4 FC matrices: TFC, KFC, PFC, and AFC (Fig. 6B). The 4 matrices (after transforming into Fisher's standardized Z variable for TFC, PFC, and AFC) were correlated with each other (linear correlation for the upper triangle) in order to examine how much they could explain of each other's variance. All above analysis was performed in 2 frequency bands: the frequency band after preprocessing (0.0067–0.5 Hz) where a low-pass temporal filter was not applied given the possible presence of meaningful signals at higher frequencies (Cole et al. 2014); and a narrower one 0.01–0.08 Hz, which has been commonly used in resting-state functional connectivity analysis (Biswal et al. 1995; Zou et al. 2008; Buckner et al. 2009).

Phase-Based Analysis

To examine whether the level of evoked activity depends on the phase of the prestimulus activity, we extracted the instantaneous phase of the BOLD signal for each ROI and each subject. This calculation was first applied to each task-run separately, and then the time-course of the instantaneous phase of each run was concatenated across the 6 task-runs.

The purposes of this phase analysis were: 1) to confirm magnitude-based analysis by comparing trials with prestimulus-trough

phase (0.5π to -0.5π) to prestimulus-peak phase (-0.5π to 0.5π), corresponding to prestimulus-low and -high magnitude, respectively; 2) to examine whether the level of evoked activity depends on whether the stimulus coincides with a rise ($-\pi$ to 0) as opposed to a fall (0 to π) of the prestimulus phases; and 3) to measure the more specific phase-dependent effect by comparing trials with prestimulus phases among 4 phase bins (Saka et al. 2010; Scheeringa et al. 2011; Yang et al. 2012): trough-fall (0.5π to π), trough-rise ($-\pi$ to -0.5π), peak-rise (-0.5π to 0) and peak-fall (0 to 0.5π). Real and pseudotrials were then grouped according to the above-defined phase ranges of prestimulus activity, respectively (Fig. 8A). The averaged raw-BOLD time-courses for these trial-groups were extracted for each ROI and each subject. Similarly to the definition of the LH index, the AUC (4–8 s) difference of the corrected-BOLD between trials with prestimulus-trough and prestimulus-peak phases (in accordance with prestimulus-low vs. -high magnitude) was defined as the Trough–Peak (TP) index. Similarly, Fall–Rise (FR) index, and Trough-Fall–Trough-Rise (TFTR) index were defined by the contrast of prestimulus-fall versus rise, and prestimulus-trough-fall versus trough-rise, respectively (Fig. 8B,C,D). Note that the TFTR index, was a confirmative measure by controlling peak and trough phases. One sample t-tests against zero at the group level were used to examine the significance of the TP, FR, and TFTR indices for each region.

As evoked activity may contaminate the phase estimate (Scheeringa et al. 2011), an additional control analysis was performed using the "background activity", that is, time-courses without evoked activity. First, the preprocessed data of each subject was inputted into a regression analysis using a customized HRF model. Specifically, we tailored our HRF model according to the observed mean BOLD response curve (Fig. 1A) to give a best fit of the evoked activity. Using AFNI function: "waver," we set the shape and duration parameters as follows: delay time (2 s), rise time (4 s), fall time (6 s), undershoot fraction (0.4), undershoot restore time (30 s), and stimulus duration (2 s). The impulse response function from waver was convolved with a square wave of the duration to make the HRF. Second, the background activity (residual data) from the regression analysis was inputted into the same phase analysis procedure as above. Third, we grouped the trials for the original time series according to the phase makers calculated from the time series of background activity (0.0067–0.5 Hz). In this way, the potential contamination of the evoked activity on phase estimates was minimized. Fourth, we recalculated all the phase-based interaction indices (TP, FR, and TFTR). Another confirmative analysis was conducted by computing all the phase-based interaction indices according to the phase makers calculated from the time series of background activity in a narrower frequency band (0.01–0.08 Hz).

Power-Law Exponent Calculation of the Spontaneous Activity

Scale-free dynamics are an intrinsic feature of many complex processes in nature, having a power spectrum following the formula $P \propto 1/f^{\beta}$, where P is power, f is frequency, and β is called the PLE indexing the degree of LRTCs (Bullmore et al. 2001; He et al. 2010). Since the variance is equal across all voxels after preprocessing, all spectra have the same integrated area. Using methods previously optimized for fMRI (Rubin et al. 2013), the resting-state data (acquired during an independent 6-min task-free fMRI scan using the same acquisition parameters) for each subject was split up into 2 halves without overlap. First, we computed the normalized power spectrum for each voxel using the AFNI program: *3dPeriodogram*, with additional smoothing in the frequency direction by 3-point linear filter ($0.15a + 0.70b + 0.15c$). Second, the power spectra of the 2 half datasets were averaged. Similar to Welch's method, this approach could reduce noise caused by imperfect and finite data, in exchange for reducing the frequency resolution. Third, the power spectra were averaged across subjects and across the 32 voxels for each ROI. In the next step, the mean power spectrum of each ROI was fitted with a power-law function $P \propto 1/f^{\beta}$ using least-square estimation in the frequency range of 0.01–0.5 Hz. The lower-frequency limit was chosen to avoid signal contributions from scanner drift (Fransson et al. 2013), whereas the higher limit on the frequency range was constrained by the sampling rate (Nyquist frequency). Lastly, the PLE of each ROI was defined as the slope of the linear regression of log-power on log-frequency corresponding to the straight-line regime (Fig. 9B). To confirm that the possible relationship between PLE and other measures was not due to any bias from frequency range selection for calculating the PLE, we repeated our calculation of the PLE from the 0.01–0.5 Hz with a lower-frequency range (0.01–0.1 Hz) (He 2011), and then performed all correlation analyses again (see below).

Phase–Amplitude Coupling of the Spontaneous Activity

Scale-free dynamics in human brain were shown to contain extensive nested frequencies in spontaneous electroencephalography (EEG or ECoG) data (Vanhatalo et al. 2004; Canolty et al. 2006; Lakatos et al. 2008; Monto et al. 2008; Tort et al. 2008; He et al. 2010). Nested frequencies refer to a systematic relationship between frequencies where the phase of lower frequencies modulates the amplitude of higher ones in an upward progression, for example, phase–amplitude coupling (PAC) (He et al. 2010).

We adopted a definition of subfrequency bands in BOLD signal (Buzsaki and Draguhn 2004; Zuo et al. 2010; Huang and Dai et al. 2014; Huang and Wang et al. 2014) including Slow5 (0.01–0.027 Hz), Slow4 (0.027–0.073 Hz), Slow3 (0.073–0.198 Hz), and Slow2 (0.198–0.5 Hz) (Fig. 9A). We applied an analogous method as in He et al. (2010) but a simplified approach for phase–amplitude coupling (PAC) in BOLD signal. Specifically, for a pair of frequencies, instantaneous phase and amplitude were extracted from the lower and higher frequencies, respectively. The lower-frequency phase across all the time points was sorted into 4 bins: trough phase (0.5π to -0.5π), peak phase (-0.5π to 0.5π), fall phase (0 to π), and rise phase ($-\pi$ to 0), which is in accordance with the above phase-based analysis during the task. Next, the concurrent higher-frequency amplitude was averaged within each bin. By comparing the higher-frequency amplitude on lower-frequency phase, the potential phase–amplitude dependence (or coupling) can be revealed. We quantified the amplitude differences of higher frequencies by contrasting TP and FR phases of lower frequencies (see Fig. 9C for an example of Slow4 and Slow3). This yielded a simplified modulation index (MI) (Tort et al. 2008; He et al. 2010) for both TP and FR, respectively. One sample t-tests against zero at the group level were used to examine the significance of MI for each region. Finally, a PAC index was defined by averaging the MI of FR in Slow5–Slow3 and Slow4–Slow3 (see Table 1 for details).

Region-Based Correlation Analyses

We sought to link trial-to-trial variability, nonadditive interaction and temporal structure of spontaneous activity. For this purpose, we first associate TTV (TTV index) and magnitude-

Table 1 Statistics of PAC in spontaneous fMRI signals

MI	Hilbert amplitude			
	Slow2 (0.198–0.5 Hz)	Slow3 (0.073–0.198 Hz)	Slow4 (0.027–0.073 Hz)	Slow5 (0.01–0.027 Hz)
Hilbert phase				
Slow2	—	—	—	—
Slow3	11 | 2	—	—	—
Slow4	3 | 6	13 | 56^{PLE}	—	—
Slow5	13 | 18	19 | 16^{PLE}	9 | 27	—

Note: In each cell: number of ROIs showing significant MI for trough versus peak phases | number of ROIs showing significant MI for fall versus rise phases. According to binomial statistics, the chance that 13, or more than 13, of 111 ROIs are individually significant at a $P < 0.05$ level is equal to $P = 0.0037$ at the population level, which is also significant after Bonferroni corrections for multiple comparisons across the 12 tests ($P = 0.044$, corrected). Numbers with superscript PLE denote significant correlation between MI and power-law exponent (PLE) across 111 ROIs. The P values of the two significant ones (MIs of FR in Slow5–Slow3 and Slow4–Slow3) are both $P < 0.001$ (also see Supplementary Table 2 for statistics). The PAC index is defined by averaging the two MIs.

based interaction (LH index) using Spearman's correlation analyses across all active ROIs, with a 95% confidence interval (CI) based on 1000 bootstrap samples (same for the following correlation analyses). This region-based approach also helps counter between-subject measurement noise (He 2011, 2013). In the second step, as a proof-of-principle, to examine whether the phase-based analysis of comparing prestimulus-trough to -peak phases (TP index) has the same performance as the magnitude-based analysis (low vs. high prestimulus magnitude, LH index), TP and LH indices were correlated. Third, we correlated the TTV index with all phase-based interaction indices (TP, FR, and TFTR) to test whether the phase-dependent effect could explain the TTV reduction. Finally, we correlated all the interaction indices (LH, TP, FR, and TFTR) with the temporal structure of spontaneous activity measured by both PLE and PAC index. In addition, the TTV index and PLE, and TTV and PAC Indices, were also correlated with each other to further confirm the observed relationship. A Bonferroni correction for multiple comparisons was performed across the above correlations.

Results

The response in 95.5% (SD = 4.5%) of the trials agreed with the a prescan questionnaire averaged across the 23 subjects. Invalid trials with unexpected responses were excluded from further analysis. Average reaction time was 590 ms (timing from questions' offset) with a SD across subjects of 363 ms.

Definition of ROIs

The activation index in 111 of the 264 putative functional areas (Power et al. 2011) was significantly above zero ($P < 0.05$, Bonferroni corrected). These active areas were defined as ROIs for the following results (Fig. 2A).

TTV Decreases Following Stimulus Onset

As expected, we observed TTV reduction following stimulus onset in widespread cortical regions (Fig. 2B). The TTV index in 40 out of 111 active ROIs was significantly below zero ($P < 0.05$, uncorrected; one sample t-tests across 23 subjects). According to binomial statistics, the chance that 11, or more than 11, of 111 ROIs are individually significant at a $P < 0.05$ level is equal to 0.023. Thus, the above results were significant at the population level ($P <$ 1e-12, binomial statistics). Our observation was well in line with previous observations (He 2013).

Magnitude-Based Interaction Across Widespread Cortical Regions

To examine if the level of evoked activity (corrected-BOLD) depends on the magnitude of the prestimulus activity (Fig. 3A), we defined the magnitude-based interaction index, LH index. In the example region, LIPL, significant interaction was seen (LH index: $P < 0.001$). Interestingly, although not significantly involved in the task ($P = 0.313$ for activation index), the RIPL (comprising the same resting-state network with LIPL) also showed significant interaction (LH index: $P < 0.001$) (Fig. 3B). The LH index in 85 of 111 ROIs was significantly above zero ($P < 0.05$), which is highly significant at the population level ($P <$ 1e-12, binomial statistics). This showed a negative interaction (He 2013) between spontaneous and evoked activity that exists in widespread cortical regions: stimuli presented at a lower magnitude of preceding spontaneous BOLD activity fluctuations produce a stronger response than stimuli presented at higher magnitude. In addition, the above results were robust, withstanding different trial sorting criteria (see Supplementary Fig. 1 for a third split approach contrasting top 33% vs. low 33%).

Comparing Our Results with the Ones by Fox et al. (2006)

Using our magnitude-based interaction analysis, we examined 4 other regions including LMC, RMC, LPAC, and RPAC. After obtaining the corrected-BOLD signal for each region, the 2 time series of prestimulus-high and prestimulus-low showed similar amplitudes, which thus seems to approximately support a linear superposition between spontaneous and evoked activity as reported previously (Fox et al. 2006). In order to go beyond mere visual inspection, we applied statistical analysis using the LH index (see above); the LH index was significant in LMC ($P = 0.006$), LPAC ($P = 0.001$) and RPAC ($P = 0.009$), and marginally significant in RMC ($P = 0.070$) which speaks in favor of a nonadditive (rather than additive) interaction (though to a modest degree) (Fig. 4).

Moreover, in order to replicate Fox et al.'s (2006) results, we used their analysis relying on co-occurring signals from homologous brain regions, that is, the activity in the homologous brain region serves as a substitute for the ongoing activity in the activated brain region. Indeed, following their method, we were unable to observe any evidence of a nonadditive interaction (as measured with LH index) either in LMC ($P = 0.780$) or LIPL ($P = 0.343$) (Fig. 5; see Supplementary Fig. 2 for a confirmation by third split). Taken together, using co-occurring signals from homologous brain regions such as RMC (Fig. 4) and RIPL (Fig. 3B) leads to different corrected-BOLD signals in LMC and LIPL in

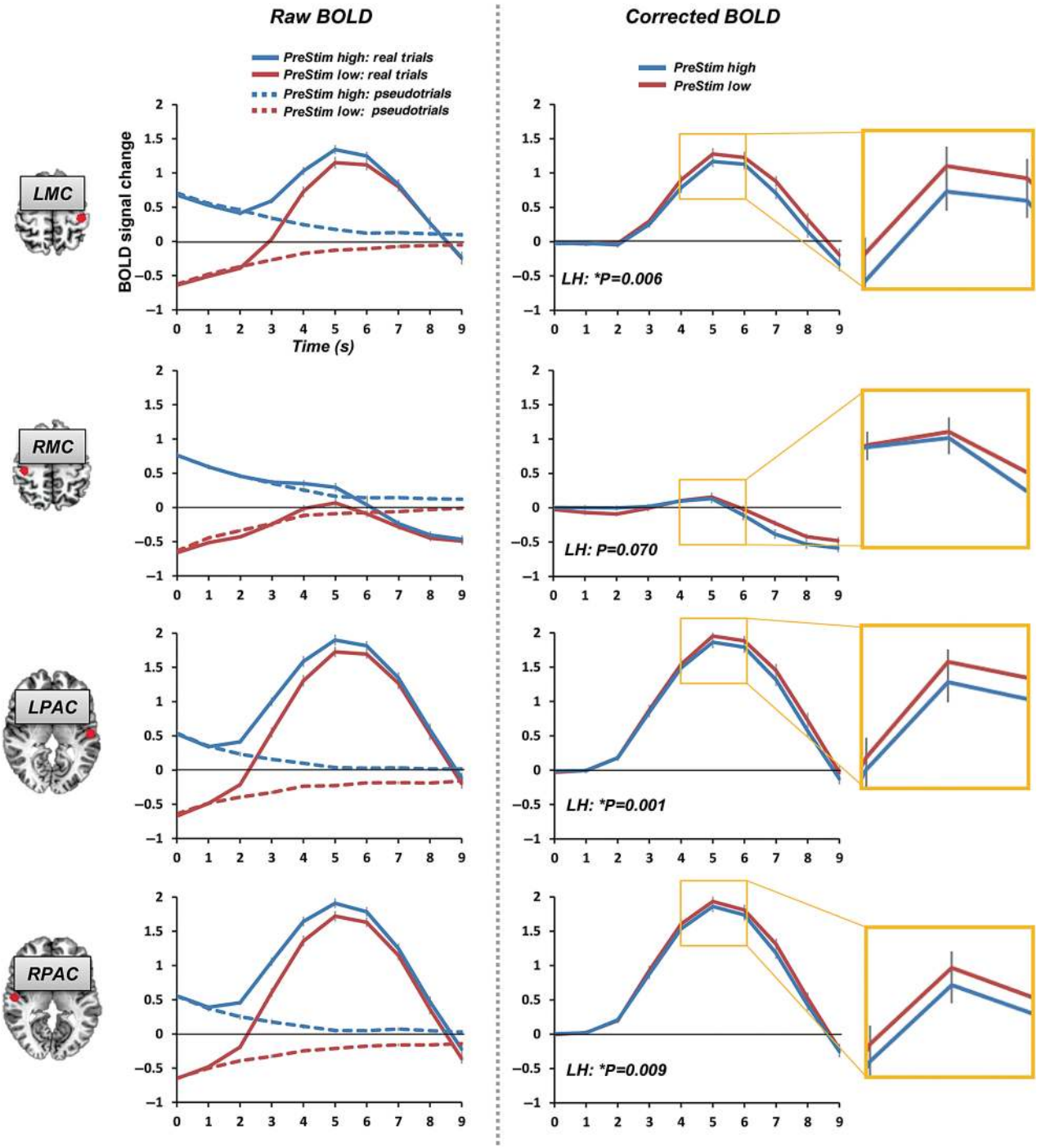

Figure 4. Magnitude-based interaction in bilateral somatomotor cortex (LMC and RMC) and primary auditory cortex (LPAC and RPAC). Although the corrected-BOLD signal of prestimulus-high and prestimulus-low showed similar amplitudes in these regions, the LH index was significant in LMC ($P = 0.006$), LPAC ($P = 0.001$), and RPAC ($P = 0.009$), and marginally significant in RMC ($P = 0.070$). Error bars indicate ±SEM.

comparison with our approach (subtracting signals of pseudotrials in the ITI).

Validation of Phase Analysis in BOLD Signal

To test whether the whole-brain functional connectivity (FC) matrices/pattern (Power et al. 2011; Cole et al. 2014) can be replicated by using Hilbert phase and amplitude, we compared 4 FC matrices (TFC, KFC, PFC, and AFC) in the resting-state data (Fig. 6). We found that all FC matrices shared a very similar pattern (Fig. 7). The correlations between TFC and all other FCs including KFC, PFC, and AFC were all significant ($P < 0.001$) in both wider (0.0067–0.5 Hz) and narrower (0.01–0.08 Hz) frequency ranges. The correlation between TFC and KFC showed the highest r values ($r = 0.992$ in 0.0067–0.5 Hz; $r = 0.986$ in 0.01–0.08 Hz), suggesting that phase synchronization analysis can replicate standard FC analysis; this validates our method of phase analysis.

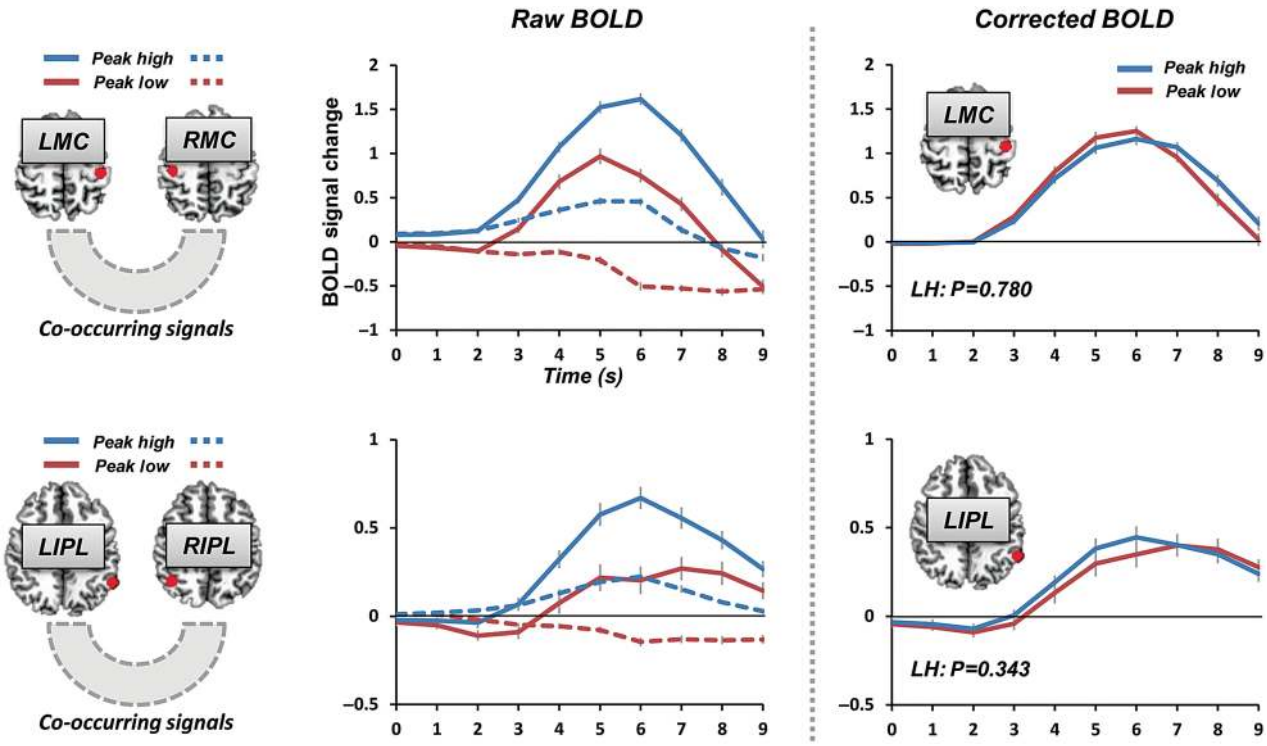

Figure 5. Replication of Fox et al.'s (2006) results. Using their method of using co-occurring signals from homologous brain regions (the activity in the homologous brain region servers as a substitute for the ongoing activity in the activated brain region), no evidence of a nonadditive interaction is found in either LMC ($P = 0.780$) or LIPL ($P = 0.343$). Error bars indicate ±SEM.

Phase-Based Interaction and Phase-Dependence

After validating the phase analysis on independent grounds (i.e., resting-state FC), we then examined whether the level of evoked activity depends on the phase of the prestimulus activity (Fig. 8*A*). We defined the TP, FR, and TFTR indices. First, using TP index, we compared trials with prestimulus-trough phase (0.5π to -0.5π) to prestimulus-peak phase (-0.5π to 0.5π), corresponding to prestimulus low and high magnitude, respectively (Fig. 8*B*). Therefore, the TP index was used to confirm the results of LH index. As expected, very similar results were observed between the TP and LH indices (Figs 8*B* and 3*B*, respectively), and the 2 indices were highly correlated ($r = 0.928$, $P < 0.001$) (Supplementary Fig. 4). This suggests the 2 indices, calculated independently, correspond to each other in terms of prestimulus low versus high magnitude and trough versus peak phases. The TP index in 82 of 111 ROIs was significantly above zero ($P < 0.05$), and was also highly significant at the population level ($P < 1e-12$, binomial statistics).

In a second step, we tested whether the level of evoked activity depends on the wave's progression (falling or rising) of prestimulus activity. We compared trials with prestimulus-fall phase (0 to π) to prestimulus-rise phase ($-\pi$ to 0), as well as prestimulus-trough-fall phase (0.5π to π) to prestimulus-trough-rise phase ($-\pi$ to -0.5π) (Fig. 8*C*,*D*; see Supplementary Fig. 3 for other regions including RIPL, LMC, RMC, LPAC, and RPAC). Interestingly, we found phase-dependent effects: the FR and TFTR indices in 26 and 12 of 111 ROIs, respectively, were significantly above zero ($P < 0.05$), and these results were also highly significant at the population level (binomial statistics, $P = 3.5e-11$ and $P = 0.0097$, respectively).

As evoked activity may contaminate the phase estimate (Scheeringa et al. 2011), an additional control analysis was performed using the "background activity" (0.0067–0.5 Hz). Our results showed that the potential contamination of evoked activity on phase estimate is negligible and all the results given above remain significant (Supplementary Fig. 5). Specifically, the TP, FR, and TFTR indices in 85, 38, and 19 of 111 ROIs, respectively, were significantly above zero ($P < 0.05$). They were also highly significant at the population level (binomial statistics, $P < 1e-12$, $P < 1e-12$, and $P = 2.6e-6$, respectively). Similar results were seen in a narrower frequency band (0.01–0.08 Hz) (Supplementary Fig. 6). In addition, no evidence was found that age or gender had an impact on these interaction indices (see Supplementary Table 1).

Taken together, these results suggest that the nonadditive interaction between spontaneous and evoked activity can be characterized by phase-dependent excitability (trough vs. peak, fall vs. rise) of spontaneous activity, with trough-fall phases showing the highest excitability.

PLE of Spontaneous Activity

The mean PLE across the ROIs was 0.92 (SD = 0.20) (Fig. 9*A*,*B* for LIPL with a PLE of 1.29). The power spectra of resting-state activity showed a linear decrease as a function of frequency, suggesting a power-law behavior for brain dynamics (He et al. 2010; He 2011).

Phase–Amplitude Coupling of the Spontaneous Activity

We examined the PAC using a simplified MI (Tort et al. 2008; He et al. 2010) in 4 subfrequency bands: Slow5 (0.01–0.027 Hz), Slow4 (0.027–0.073 Hz), Slow3 (0.073–0.198 Hz), and Slow2 (0.198–0.5 Hz) (see Fig. 9*C*). For the contrast of trough versus peak phases, significant MIs in Slow5–Slow3, Slow5–Slow2, and Slow4–Slow3 were found; and for the contrast of fall versus rise, significant MIs in Slow5–Slow4, Slow5–Slow3, Slow5–Slow2, and Slow4–Slow3 were

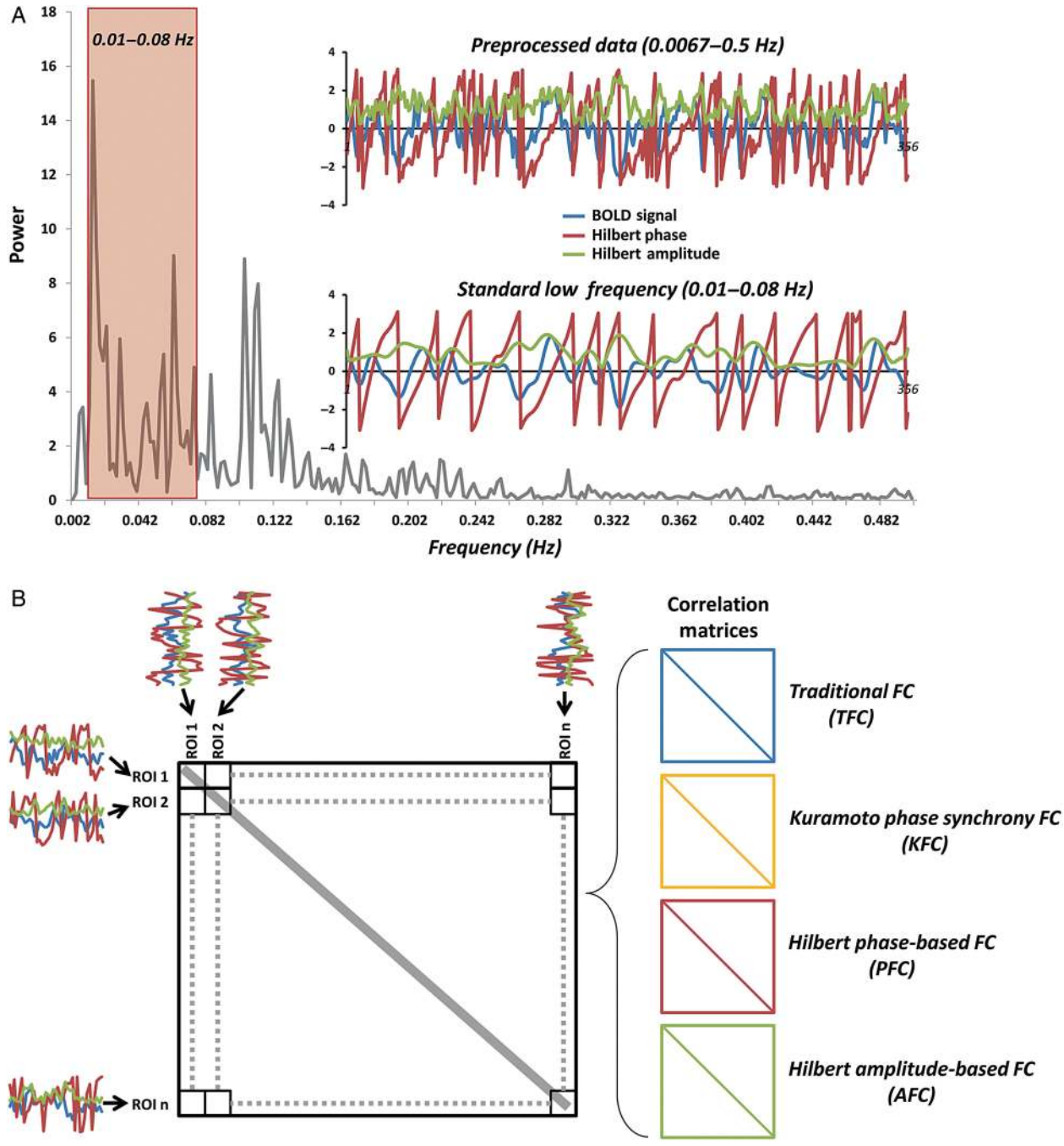

Figure 6. Illustration of Hilbert phase analysis and its validation in spontaneous fMRI signals (acquired during an independent 6 min task-free fMRI scan). (*A*) The power spectrum of an example time series in LIPL from Subject 08. The BOLD time series in two frequencies (0.0067–0.5 Hz and 0.01–0.08 Hz) and their instantaneous phase and amplitude traces (by Hilbert transform) are shown in the upper-right. (*B*) Four FC matrices were calculated: TFC, KFC, PFC, and AFC. For the TFC, Pearson correlation analysis was performed for a given pair of BOLD time series from two nodes. For the KFC, the averaged phase synchrony across time was calculated between a given pair of phase series from two nodes (see Materials and Methods for details). For the PFC, similarly to the TFC analysis which uses Pearson correlation, the PFC matrix was computed based on the Hilbert phase series instead of the BOLD signal itself. In a similar way, the AFC matrix was computed based on the Hilbert amplitude series using Pearson correlation.

seen (Table 1). Additionally, the MIs of Slow5–Slow3 and Slow4–Slow3 in fall versus rise showed significant correlations with PLE across 111 ROIs ($P < 0.001$; see Supplementary Table 2). The MIs of Slow5–Slow3 and Slow4–Slow3 in fall versus rise were also correlated with each other ($r = 0.28$, $P = 0.003$). For that reason, we collapsed both MIs yielding a PAC index for each ROI in all subsequent correlation analyses (see below).

The Relationship Between TTV Index, Interaction Indices, PLE, and PAC Index

Linking trial-to-trial variability, nonadditive interaction and temporal structure of spontaneous activity, we first visualized all indices according to their value ranking across the 111 active ROIs in the brain (Fig. 10). We found that the magnitude-based

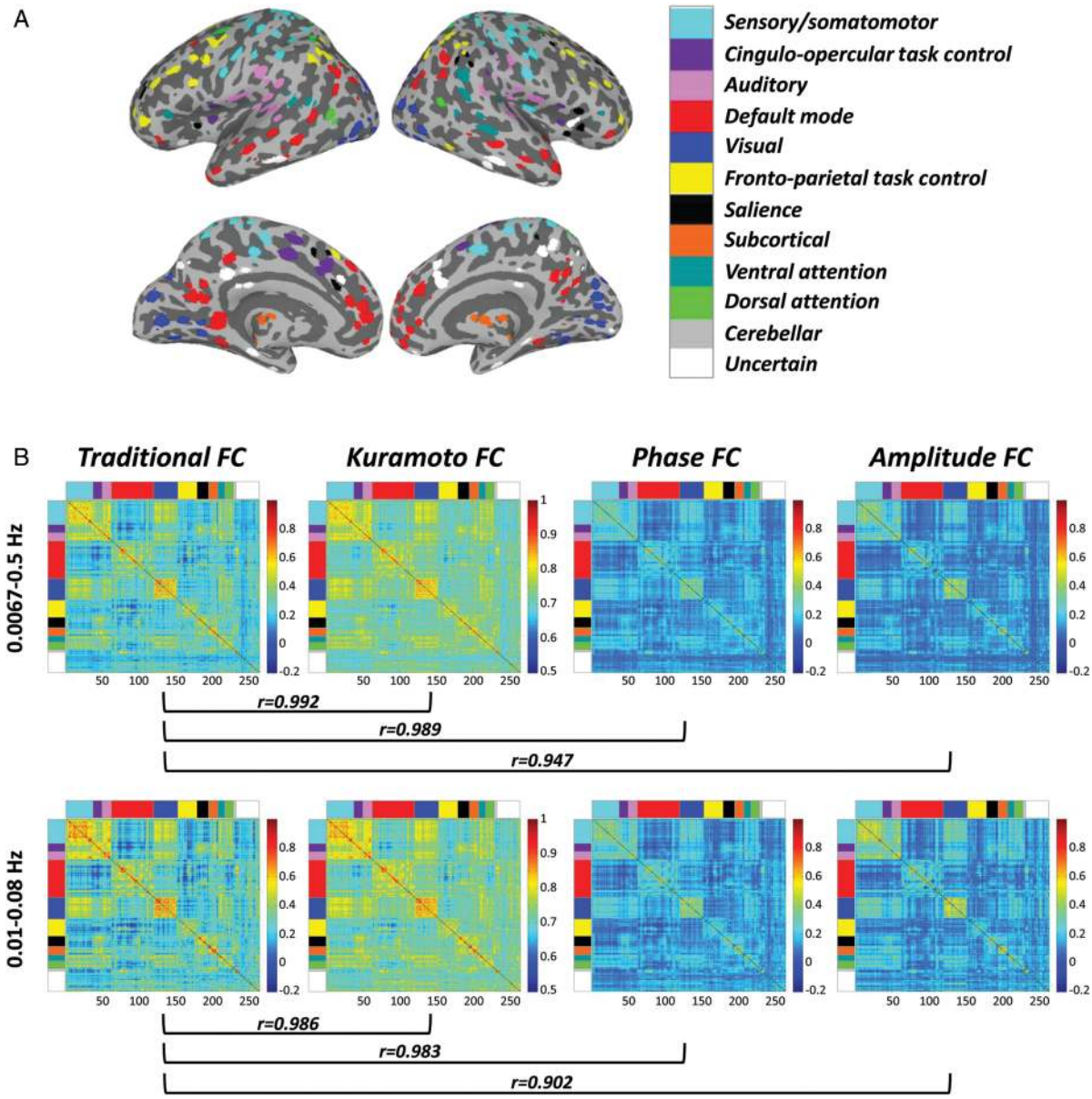

Figure 7. The validation of Hilbert phase analysis in BOLD signal with a predefined node template (Power et al. 2011; Cole et al. 2014). (*A*) The node template is visualized in an inflated brain with eleven distinct networks plus uncertain regions (Cole et al. 2014). (*B*) Four FC matrices of spontaneous fMRI signals (6 min task-free fMRI scan) are presented: TFC, KFC, PFC, and AFC. These FC matrices shared a very similar pattern, where the correlations between TFC and all other FCs including KFC, PFC, and AFC were all significant ($P < 0.001$) in both wider (0.0067–0.5 Hz) and narrower (0.01–0.08 Hz) frequency ranges. This serves as validation of phase analysis on the basis of traditional functional connectivity.

interaction index (LH), phase-based interaction indices (TP, FR, and TFTR), PLE and PAC index shared a similar spatial distribution pattern, and the TTV index showed the opposite. Moreover, we observed concordant gradient changes in relation to the LH index in all 3 phase-based interaction indices, PLE and PAC index, along with an opposite gradient change in the TTV index (Fig. 11).

The above relationship was further examined by correlating the TTV index, PLE, and PAC index with all interaction indices (LH, TP, FR, and TFTR), as well as correlating between TTV index, PLE, and PAC index. The analyses were performed using Spearman's correlations across 111 ROIs. The results showed that the TTV index and all interaction indices were negatively correlated (TTV-LH: $r = -0.60$; TTV-TP: $r = -0.53$; TTV-FR: $r = -0.67$; TTV-TFTR: $r = -0.49$), while all interaction indices and the PLE were positively correlated (LH-PLE: $r = 0.70$; TP-PLE: $r = 0.66$; FR-PLE: $r = 0.38$; TFTR-PLE: $r = 0.31$). All interaction indices and PAC index were also positively correlated (LH-PAC: $r = 0.48$; TP-PAC: $r = 0.44$; FR-PAC: $r = 0.42$; TFTR-PAC: $r = 0.32$). As expected from the above observations, the TTV index and PLE were negatively correlated ($r = -0.56$), the TTV index and PAC index were negatively correlated ($r = -0.43$), and the PLE and PAC index were positively correlated ($r = 0.53$) (see Fig. 12 for a summary; Supplementary Table 3 for all statistics). The significance for all above correlations was $P < 0.001$, which was significant enough to survive a Bonferroni correction for multiple comparisons.

Several additional correlation analyses were used to confirm the above results. First, for the magnitude-based interaction

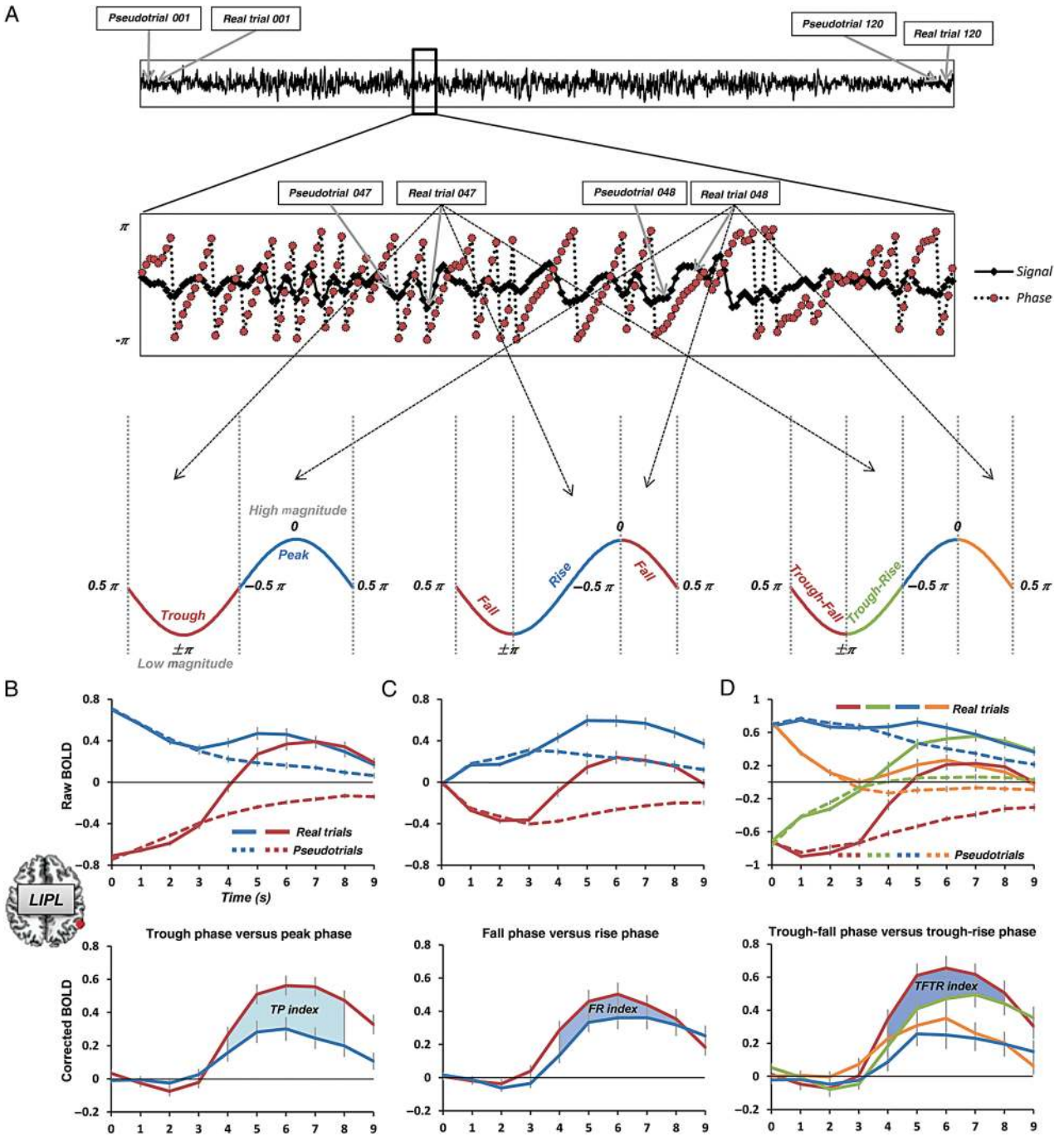

Figure 8. Illustration of phase-based analysis and phase-dependent effect of fMRI signal (LIPL as an example). (*A*) All trials for each subject were grouped according to the phase markers of prestimulus activity. This approach was performed on real and pseudotrials independently. (*B*) Confirming the magnitude-based analysis (LH index), very similar results were seen when comparing trials with prestimulus-trough phase (0.5π to -0.5π) to prestimulus-peak phase (-0.5π to 0.5π) by TP index (AUC 4–8 s, same as follows). (*C*) Comparing trials with prestimulus-fall phase (0 to π) to prestimulus-rise phase ($-\pi$ to 0) by FR index, the level of evoked activity was shown to be dependent on the wave's progression (falling or rising) of prestimulus activity. (*D*) The phase-dependent effect was further confirmed (controlling peak and trough phases) by comparing trials with prestimulus-trough-fall phase (0.5π to π) to trough-rise phase ($-\pi$ to -0.5π) as measured by TFTR index. Error bars indicate ±SEM.

index (LH), we confirmed that the above correlations were robust to different trial sorting criterions (see Supplementary Table 4: third split contrasting top 33% vs. low 33%). Second, we repeated our calculation of the phase-based indices (TP, FR, and TFTR) using the "background activity" in both wider (0.0067–0.5 Hz) and narrower (0.01–0.08 Hz) frequency bands. The above correlation remains significant (see Supplementary Table 5). Third, to avoid any bias from frequency range selection for calculating the PLE, we repeated our calculation of the PLE from 0.01–0.5 Hz with a narrower frequency range (0.01–0.1 Hz) as suggested in a previous study (He 2011). Again, the above correlations remain significant (see Supplementary Table 6). Lastly, the temporal variance (TV) was reported to have a close relationship with the PLE (He 2011); we also examined the correlations between the

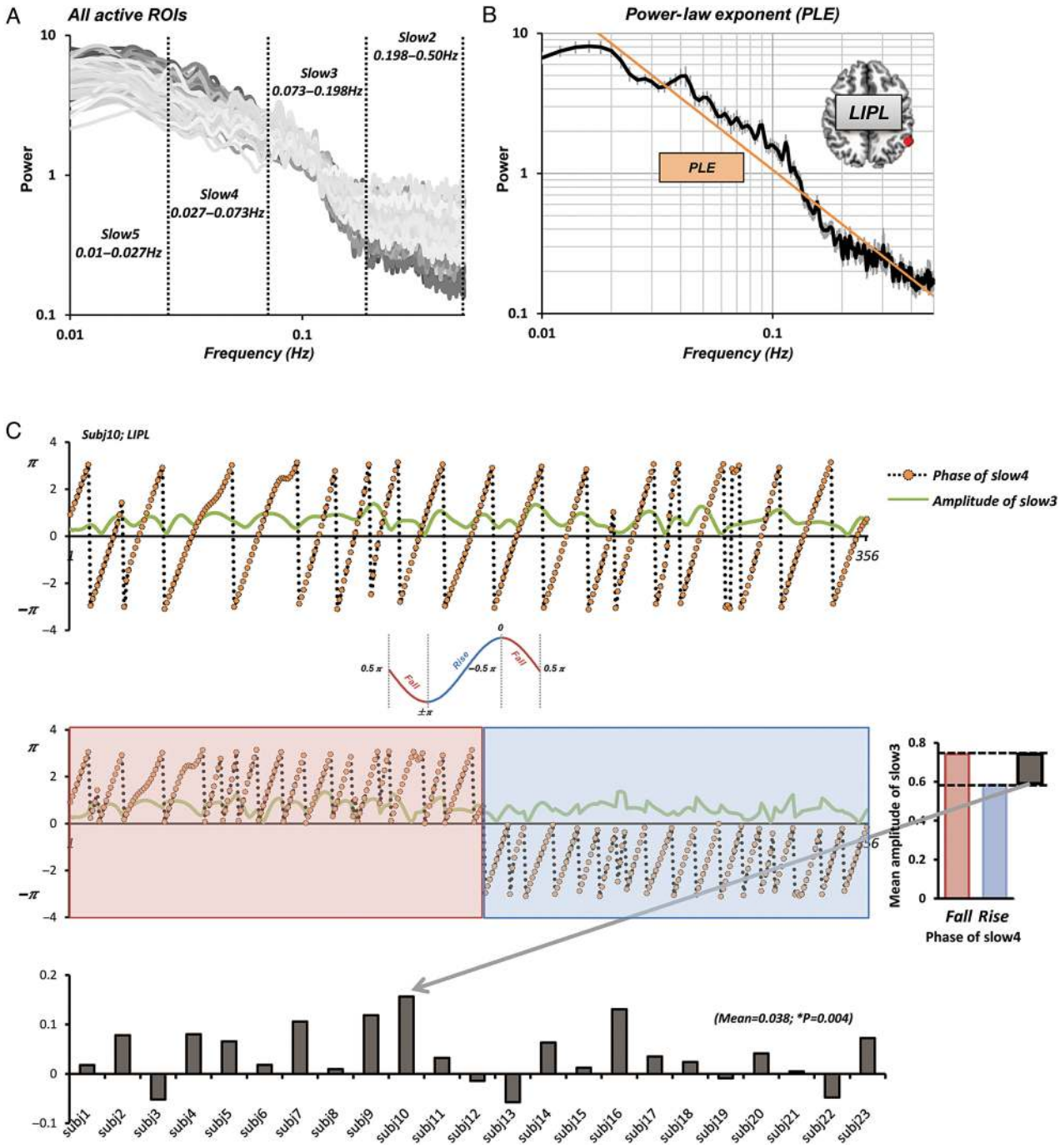

Figure 9. Power spectra, PLE and PAC. (*A*) Power spectra of spontaneous fMRI signals (6 min task-free fMRI scan) for all ROIs. Subfrequency bands in BOLD signal, including Slow5 (0.01–0.027 Hz), Slow4 (0.027–0.073 Hz), Slow3 (0.073–0.198 Hz), and Slow2 (0.198–0.5 Hz) are shown (Zuo et al. 2010). (*B*) The power-law exponent (PLE), β, was defined as the slope of a linear regression of log-power on log-frequency corresponding to the straight-line regime (LIPL as an example). (*C*) For a pair of frequencies (Slow4 and Slow3 for this example; BOLD signal from LIPL of subject 10), instantaneous phase and amplitude were extracted for the lower (Slow4) and higher (Slow3) frequencies, respectively. The amplitude differences of higher frequencies were calculated by contrasting trough versus peak (TP) and rise versus fall (FR) phases of lower frequencies (FR for this example). This yielded a simplified MI (Tort et al. 2008; He et al. 2010) for both TP and FR, respectively. One sample *t*-tests against zero at the group level were used to examine the significance of MI for each region. Significant MI of Slow4–Slow3 FR at the group level was seen in the LIPL for this example.

temporal variance—in both resting state and ITI—and all other indices. As expected, significant correlation was found between TV and PLE. In addition, the TV also correlated with other indices (TTV, LH, TP, FR, and TFTR) but not the PAC index (see Supplementary Table 7).

Discussion

Using an extremely sparse event-related design (ITIs from 52 to 60 s), a novel correction approach, and phase analysis of fMRI signals, we demonstrate that 1) stimuli presented at a lower magnitude of preceding spontaneous BOLD activity fluctuations

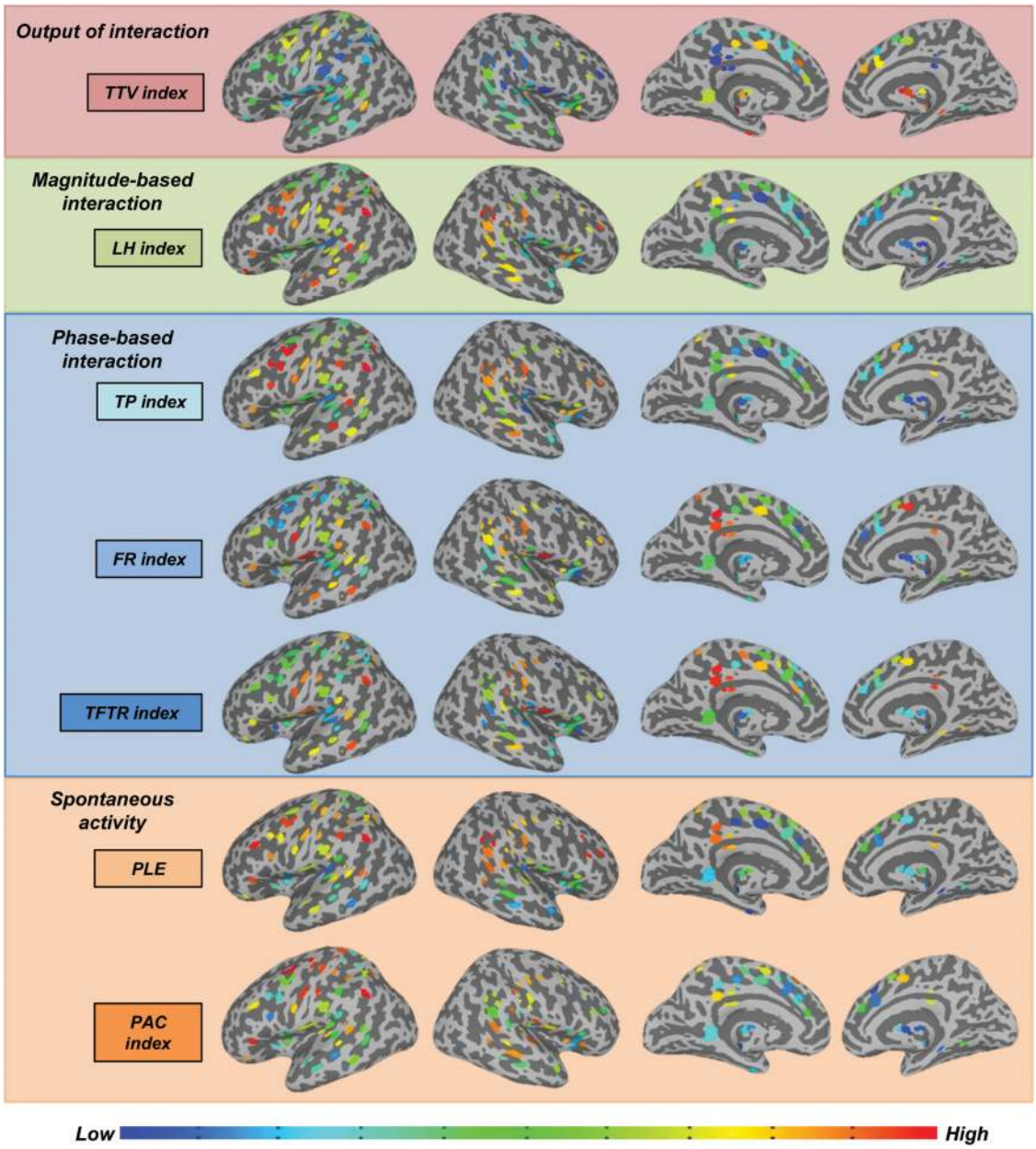

Figure 10. Visualization of all indices according their value ranking across the 111 ROIs from low to high. The magnitude-based interaction index (LH), phase-based interaction indices (TP, FR, and TFTR), PLE and PAC index all shared a similar spatial distribution pattern, and the TTV showed the opposite. TTV, trial-to-trial variability; LH, low–high; TP, trough–peak; FR, fall–rise; TFTR, trough-fall–trough-rise; PLE, power-law exponent; PAC, phase–amplitude coupling.

produce a stronger response than stimuli presented at a higher magnitude, which explains trial-to-trial variability reduction after stimulus-onset; 2) the discrepancy between the results presented here (nonadditive interaction) and previous observations (linear superposition) (e.g., Fox et al. 2006) is due to different assumptions about spontaneous activity and methods of analysis in obtaining corrected-BOLD signal; 3) the nonadditive interaction can be characterized by phase-dependent excitability of spontaneous activity. That is, different levels of excitability can be seen in trough versus peak and fall versus rise phases, where trough–fall phases show the highest excitability; 4) the degree of the phase-dependent excitability is related to the degree of the LRTCs in spontaneous activity, as indexed by both power-law exponent and phase–amplitude coupling.

Nonadditive Interaction

Several studies reported that prestimulus spontaneous activity has an impact on behavioral performance (Boly et al. 2007; Fox and Raichle 2007; Hesselmann, Kell and Eger et al. 2008; Hesselmann, Kell and Kleinschmidt 2008; Sadaghiani et al. 2009, 2010; Northoff et al. 2010). However, these studies did not quantitatively demonstrate an interaction between spontaneous and evoked activity. Recently, a negative interaction between the 2 activities was proposed based on an indirect observation, namely, a decreased TTV after stimulus-onset, which is considered a consequence of the negative interaction (He 2013). The phenomenon of TTV reduction was also reported in ECoG (He and Zempel 2013) and neuronal firing on the cellular level (Churchland et al.

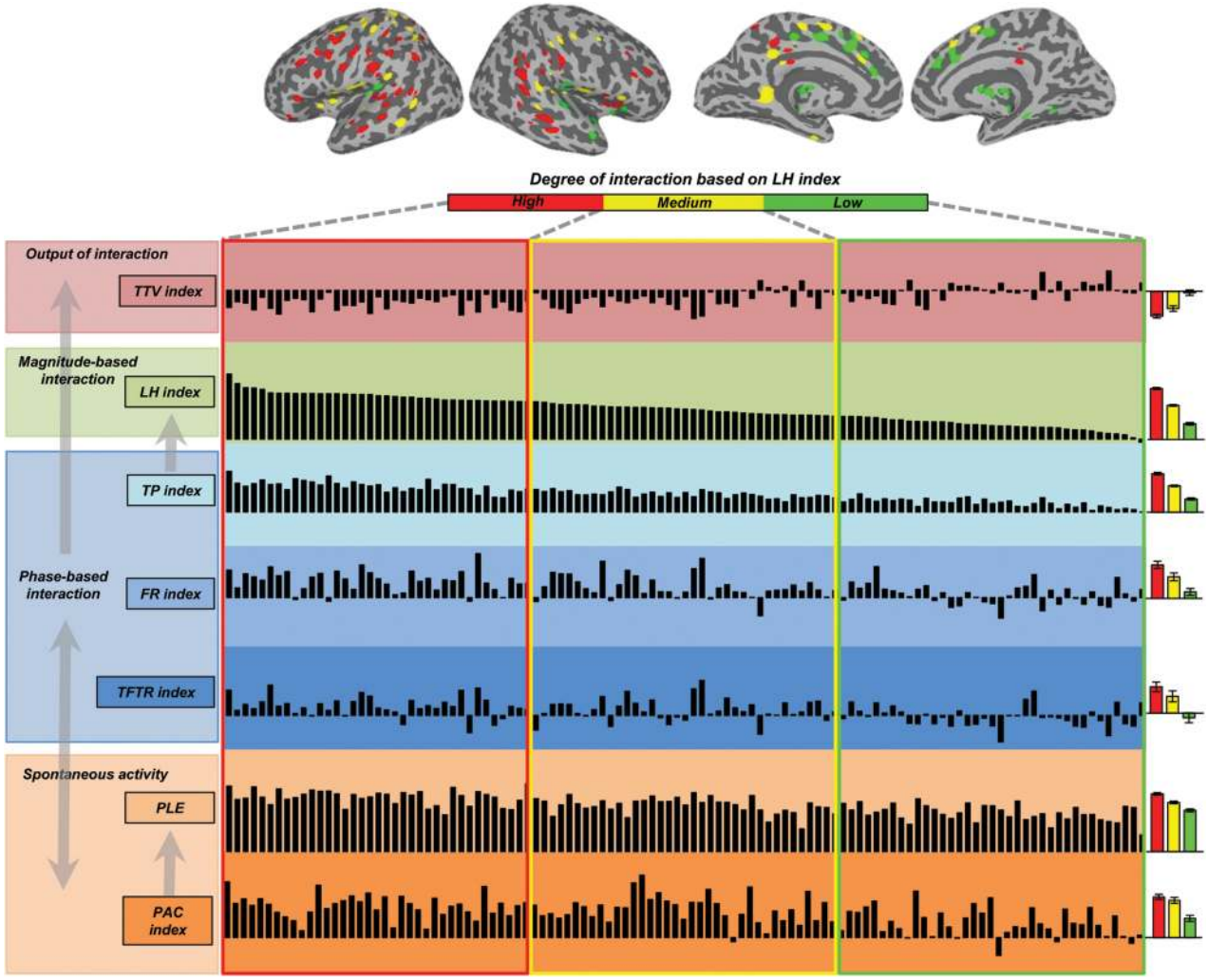

Figure 11. Visualization of the LH index across ROIs in relation to the TTV index, phase-based interaction indices (TP, FR, and TFTR), PLE and PAC index. The 111 ROIs were sorted based on the value of the LH index into 3 groups: high, medium and low (37 ROIs for each group). Other indices as well as the PLE were presented in the same order. By averaging these measurements in corresponding ROIs' groups (bars on the right with mean and SEM across regions), concordant gradient changes in relation to the LH index were seen in all 3 phase-based interaction indices (TP, FR, and TFTR), PLE and PAC index, along with an opposite gradient change was found in the TTV index. TTV, trial-to-trial variability; LH, low–high; TP, trough–peak; FR, fall–rise; TFTR, trough-fall–trough-rise; PLE, power-law exponent; PAC, phase–amplitude coupling.

2010; Chang et al. 2012; White et al. 2012). In addition, the behavioral relevance of TTV has also been shown in EEG-MEG (Schurger et al. 2015), EEG-fMRI (Mayhew et al. 2013), fMRI (He 2013), ECoG (He and Zempel 2013), and intracellular recoding (Carandini 2004; Marcos et al. 2013; Churchland et al. 2010; Scaglione et al. 2011). The TTV in membrane potentials of visual cortical cells decreases in response to high contrast stimuli, which is suggested to be a key mechanism that allows the nervous system to disambiguate stimulus strength from attribute (Finn et al. 2007). Nevertheless, future validations of the TTV method across different modalities (intracellular recoding, EEG, MEG, and fMRI), as well as revealing its underlying physiological mechanism, remain to be addressed.

Importantly, extending these observations, our findings provide direct evidence and straightforward measures of the nonadditive interaction between spontaneous and evoked activity. Using a magnitude-based interaction index (LH) to compare trials with prestimulus-high magnitude to those with prestimulus-low magnitude (after BOLD correction), we observed a relatively stronger evoked BOLD response when the stimulus was presented at lower prestimulus magnitude of spontaneous activity in almost all the active regions. As expected, the LH index correlated with the TTV index, which helps confirm the prediction of the negative interaction (He 2013). Despite the fact that different tasks were used and thus different sensory modalities were recruited, our current study (auditory semantic-judgment task) together with He's study (He 2013) (visual detection) strongly contradict the linear superposition model proposed and elaborated in the past 2 decades (Arieli et al. 1996; Azouz and Gray 1999; Fox et al. 2006; Becker et al. 2011).

Methodologically, our long ITI's experimental design and fMRI signal correction approach (accounting for spontaneous fluctuations using pseudotrials) allowed us to provide the aforementioned evidence. It is important to note that we did not assume that the spontaneous activity modeled by pseudotrials was identical to that which underlies real trials. First, theoretically, it is impossible to directly dissociate spontaneous and evoked activity from the recorded signal, as the spontaneous activity may continue to vary after stimulus onset. Second, the distinction itself must be put into doubt once linear superposition no

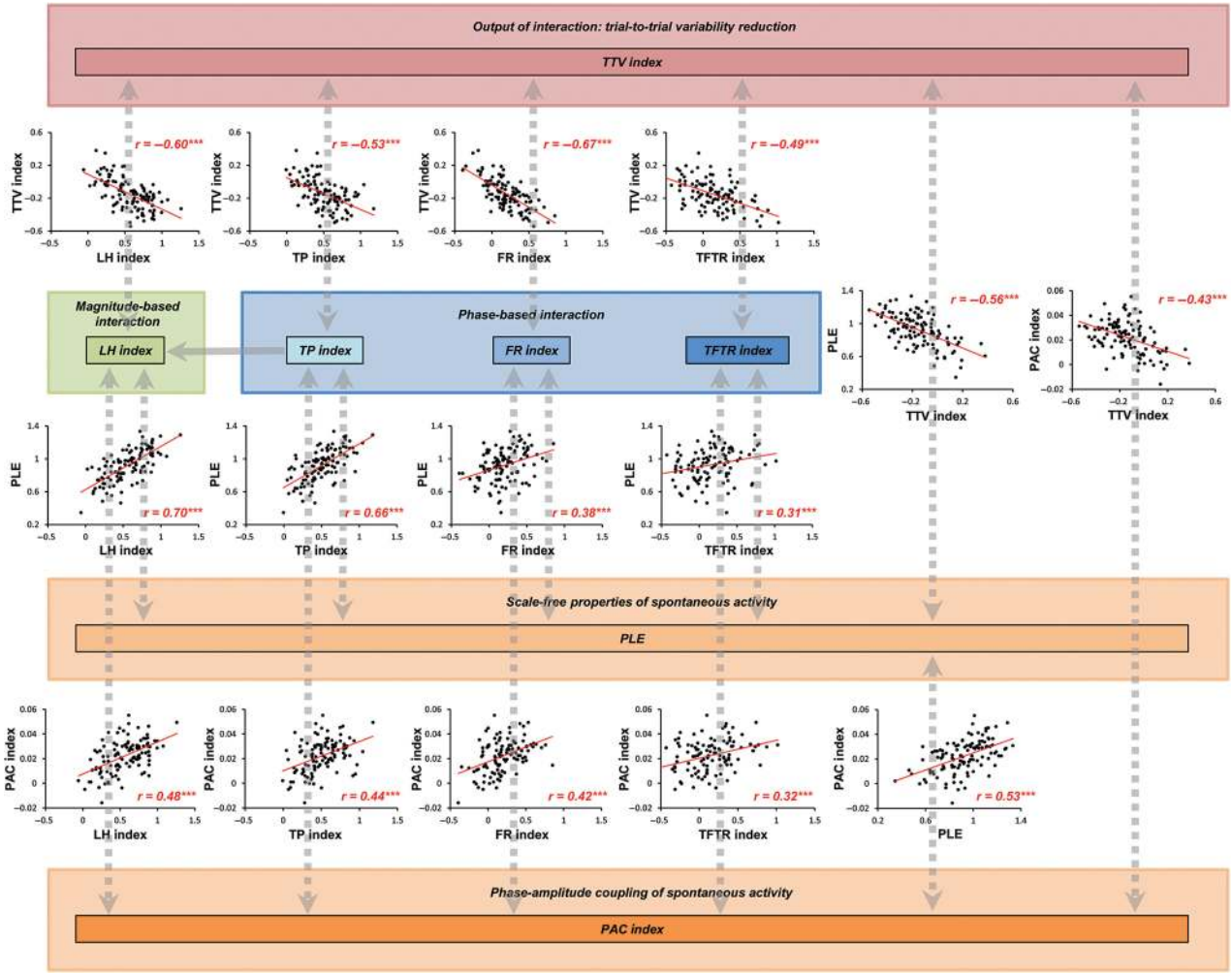

Figure 12. The relationship between the TTV index, interaction indices (LH, TP, FR, and TFTR), PLE and PAC index. The correlation analyses were performed using Spearman's correlations across 111 ROIs, with a 95% CI based on 1000 bootstrap samples. The significance for all above correlations is $P < 0.001$ (denoted by ***), which is significant enough to survive a Bonferroni correction for multiple comparisons. TTV, trial-to-trial variability; LH, low–high; TP, trough–peak; FR, fall–rise; TFTR, trough-fall–trough-rise; PLE, power-law exponent; PAC, phase–amplitude coupling.

longer holds. Lastly, in taking the view that the brain is a dynamic system that selects its trajectory based on the context and adjusts that trajectory when performing a task (He 2013), the spontaneous activity modeled by the pseudotrials in our study should represent what would have been the spontaneous activity if the task was not performed. In this sense, the interaction indices defined in our study, based on the contrast of real- versus pseudotrials, can be considered to indicate how the incoming stimuli modulate the brain's spontaneous activity in a manner that depends on the brain's initial state (at stimulus onset).

We also validated our results in a few regions involved and not involved in the task, including bilateral inferior parietal lobule (LIPL and RIPL), somatomotor cortex (LMC and RMC) and primary auditory cortex (LPAC and RPAC). Using our approach, obtaining corrected-BOLD signals by subtracting pseudotrials during the ITI, all regions showed significant nonadditive interaction (except for RMC that showed marginal significance). Note that the corrected-BOLD signals of prestimulus-high versus prestimulus-low in LMC, RMC, LPAC and RPAC indeed showed similar amplitudes. These sensory cortical regions (e.g., somatomotor and auditory) thus seem to show a rather modest degree of nonadditive interaction, which visually accords with an "approximately" linear superposition between spontaneous and evoked activity as observed previously (Fox et al. 2006).

Why then is there a discrepancy between our findings of nonadditive interaction and the earlier report (Fox et al. 2006), which suggested a linear superposition between spontaneous and evoked activity? We replicated Fox et al.'s (2006) results using their approach achieved by co-occurring signals from homologous brain regions assuming that they are not influenced by the task. Following their method, we were also unable to observe any evidence of a nonadditive interaction. However, as shown above, the homologous brain regions (RIPL and RMC) nevertheless exhibit an observable nonadditive interaction effect (Figs 3B and 4). This suggests that these regions were in fact influenced by the task, so that they may not represent proper ongoing activity that is unaffected by the task, which Fox et al. (2006) assumed (see a similar argument based on the TTV reduction in RMC in He 2013). Therefore, we conclude that by subtracting the co-occurring signals from the homologous regions (e.g., RIPL and RMC), one cancels out the nonadditive interaction effect in the active regions (e.g., LIPL and LMC), which leads to the observation of a linear superposition between spontaneous and evoked activity.

Phase-Dependent Excitability

What is the mechanism underlying this nonadditive interaction? Here we propose a candidate mechanism, phase-dependent excitability, observed in our phase-based interaction indices (TP, FR, and TFTR) as well as their relationship to the TTV index. As is known, the dominant oscillatory spontaneous brain activity in fMRI during resting wakefulness is observed in frequencies lower than 0.5 Hz and it is commonly referred to as the slow cortical potential or infraslow fluctuation (He and Raichle 2009). These fluctuations have been suggested to be crucial for normal brain functioning (Raichle and Mintun 2006; Fox and Raichle 2007; He et al. 2007; Luczak et al. 2009; Berkes et al. 2011; He 2013) but their exact functional role remains unknown. Our observations suggest that the phase cycle of the infraslow fluctuations contains different levels of "temporal excitability" for subsequent stimuli (Palva and Palva 2012). Stimulus responses at time points of reduced excitability would be expected to be lower than responses at points in the cycle of increased excitability. In other words, the spontaneous activity's ongoing phase cycles modulate the effectiveness of the external stimulus/task, which in turn yield different levels of evoked activity and behavioral outcomes, and explain the observed trial-to-trial variability reduction of evoked activity after stimulus-onset. Our proposed phase-dependent excitability is in line with the "state-dependent network model"; based on computational modeling, ongoing activity and its temporal excitability can be regarded as a state-dependent spatiotemporal property that impacts the processing of stimuli (Buonomano and Maass 2009).

Alternatively, since our data were based on fMRI signals, the nonadditive interaction may be seen in the context of another phenomenon called the BOLD saturation or ceiling effect (Haller et al. 2006; Goebel and Van Atteveldt 2009). However, we deem this effect an unlikely explanation for 2 reasons: 1) if the interaction between spontaneous and evoked activity is just due to BOLD saturation effect at prestimulus, one would expect to see identical evoked activity for an identical saturation level (identical magnitude) of prestimulus activity. However, this was not the case in our data when comparing trials with prestimulus rise and fall phases (Fig. 8*C* and Supplementary Fig. 7); 2) if the interaction is just due to BOLD saturation effect during the peak period, one would expect to see higher evoked activity for a lower saturation level (lower magnitude) during the peak period. However, our data showed the opposite when comparing trials with prestimulus-trough-rise to trials with prestimulus-peak-fall phases (Fig. 8*D* and Supplementary Fig. 7).

Nonadditive Interaction and the Temporal Structure of Spontaneous Activity

Consistent with previous studies, our results showed that spontaneous fMRI signals during resting-state display rich temporal organization (LRTCs) across widespread cortical regions as indexed by their scale-free $1/f^{\beta}$ power spectra (Bullmore et al. 2001; Linkenkaer-Hansen et al. 2001; He et al. 2010; He 2011; Palva et al. 2013). Such LRTCs are shared by many systems found in nature (Chialvo 2010; He et al. 2010) and, most importantly, have also been observed in neural activity across many different spatiotemporal scales: from neurotransmitter release (Lowen et al. 1997), neuronal spike trains (Lowen et al. 2001), network firing rates (Garcia-perez et al. 2007), field potentials (Linkenkaer-Hansen et al. 2001; Manning et al. 2009; Miller et al. 2009; He et al. 2010; Palva et al. 2013), to fMRI signals (He et al. 2010; He 2011).

Our results extend the current literature by showing that the degree of LRTCs, as indexed by the power-law exponent, in spontaneous brain activity of the resting-state (independently to the performed task) is related to the degree of the phase-dependent effect between spontaneous and evoked activity during the task; the higher the degree of LRTCs (larger power-law exponent) in spontaneous activity, the larger the degree of the phase-dependence effect and the subsequent TTV reduction. This suggests that LRTCs in spontaneous activity have an impact on the degree to which the spontaneous activity interacts with the stimuli or task. In other words, a change in the power-law exponent implies a change in the nonadditive interaction. If the spontaneous brain activity were only white noise (power-law exponent = 0), then one would get a pure additive activity. Once the internal activity starts being auto-correlated (begins to form memory of the past) then the interaction turns to be nonadditive or nonlinear (see below for further discussion between "nonadditive" and "nonlinear"). Finally, although we obtained our data based on BOLD-fMRI, our findings potentially have important implications for activation properties at a cellular level, where LRTCs and TTV reduction have also been observed (Lowen et al. 2001; Garcia-perez et al. 2007; Churchland et al. 2010; White et al. 2012).

How could LRTCs within spontaneous activity modulate the phase-dependent excitability? As suggested in a previous study, scale-free dynamics can be characterized by nested frequencies in which a particular phase of the lower-frequency fluctuation could modulate the activity of higher frequencies (He et al. 2010). For instance, the trough of surface-recorded slow cortical potentials (SCPs), which constitute the low-frequency end of the $1/f^{\beta}$ power spectrum (Monto et al. 2008; He and Raichle 2009), is associated with increased cortical excitability and an increased amount of higher-frequency activities (Vanhatalo et al. 2004; He and Raichle 2009).

Nested frequencies have been observed in spontaneous EEG (or ECoG) data (Vanhatalo et al. 2004; Canolty et al. 2006; Lakatos et al. 2008; Monto et al. 2008; Tort et al. 2008; He et al. 2010), whereas they remain poorly investigated in fMRI data. This may be partly due to the relatively low temporal resolution in fMRI on the one hand, and less consensus in the literature on the definition of sub-frequencies in BOLD signals on the other hand. However, as an exploratory investigation, we have extended previous observations from EEG/ECoG to fMRI signals by showing widespread nested frequencies across brain regions in Slow5 (0.01–0.027 Hz), Slow4 (0.027–0.073 Hz), Slow3 (0.073–0.198 Hz), and Slow2 (0.198–0.5 Hz), measured by a simplified MI (Tort et al. 2008; He et al. 2010). The links between nested frequencies and scale-free properties were found in the MIs of Slow5–Slow3 and Slow4–Slow3 in fall versus rise, where the MIs showed significant correlations with the PLE. Furthermore, the PAC index (collapsing the MIs of Slow5–Slow3 and Slow4–Slow3 in fall vs. rise) was also highly correlated with all the interaction indices.

Taken together, we tentatively propose that the LRTCs within spontaneous activity may impact the phase-dependent excitability via intrinsic phase–amplitude coupling. We acknowledge that our choice of phase bins ($\pi/2$) for phase–amplitude coupling analysis may be somewhat arbitrary and coarse-grained, since it may not capture the fine-grained temporal organization as shown in EEG and ECoG studies (e.g., He et al. 2010). In addition, we found the PAC in rise versus fall phases shows the strongest correlation with the scale-free properties (e.g., PLE); however that leaves open the question of why we did not obtain such correlations in peak versus trough phases. Future studies combining EEG, MEG, and fMRI to target both higher-frequency and

infraslow-frequency bands are required to confirm and expand upon the observation.

Limitations and Methodology Issues

We demonstrated that spontaneous and evoked activity interact in a nonadditive, rather than additive or linear superimposed, way. Under the umbrella term "nonadditive," 2 possible scenarios can be taken into account for the relationship of spontaneous and evoked activity. That is, the evoked activity (corrected-BOLD signal) may change as a function of prestimulus spontaneous activity in 1) a linear way or 2) a nonlinear way. If the former is true, one would expect that trials with different levels of prestimulus activity should correspond to different levels of evoked activity. However, the phase-dependence effect revealed by our data invalidates this assumption, as the evoked activity can be different when the prestimulus activity is the same (e.g., comparing trials with prestimulus-rise to trials with prestimulus-fall phases; Fig. 8C). Another counter-example for the linear scenario was provided by an analysis using 8-split of trials based on both prestimulus magnitude and prestimulus phases in the LIPL (Supplementary Fig. 8). Our results remain in favor of a nonlinear relationship. Nevertheless, we are unable to provide an exact nonlinear relationship between spontaneous and evoked activity, as phase-dependence of the fMRI signal may pertain to as of yet unclear nonlinear mechanisms, especially considering the complex relationship from neural activity on the cellular level to hemodynamic response on the regional level. Thus, at this point, we chose to use the broader term "nonadditive" instead of "nonlinear" to describe the above relationship. This issue of nonlinear mechanisms may be potentially addressed by future studies combining neural modeling, neuroimaging and electrophysiology.

Our results argue for a refining of traditional general linear models (GLM) as well as experimental designs that take spontaneous fluctuations of brain activity, including its ongoing phases, more accurately into account. For example, one may want to compare different event categories presented using a (pseudo) randomized event-related fMRI design. If the number of trials is not sufficient, and by coincidence the stimuli of the different event categories fall into different prestimulus ongoing phases, one may obtain different estimated activations using GLM analysis for the different event categories. However, this may simply be due to the differences in prestimulus phases rather than the different event categories themselves. In an extreme example, this could be true even for presenting pseudotrials without actual stimuli (see Supplementary Fig. 9 for an illustration). Collectively, insufficient number of trials may give rise to false-positive results deriving from unbalanced prestimulus phases. Stepping back from this extreme example, one may assume that the number of trials for different event categories is sufficient. This, to some extent, could minimize the potential confound of prestimulus phases, albeit not fully exclude it. There is at least one scenario which has not been taken into account in the traditional GLM analysis: while different event categories have the same estimated activation, they may have different degrees of phase-dependent interaction and hence different TTV after stimulus-onset as shown previously (Fig. 4*B* in He 2013). Taken together, however, it remains to be determined 1) how to optimize an fMRI design to reduce the potential confound of prestimulus phases; 2) how an interaction effect between spontaneous and evoked activity could be integrated within a GLM framework.

While phase analysis (e.g., Hilbert transform in our study) is relatively well-established in EEG research (Le Van Quyen et al. 2001; Le Van Quyen and Bragin 2007; Monto et al. 2008; Yang et al. 2012), it is important to interrogate if this analysis is sensible for the BOLD signal. This has been explored only in a handful of fMRI studies. Laird et al. (2002) applied this analysis to identify synchronization of BOLD responses during a finger tapping experiment. They demonstrated the potential of the method compared with the traditional GLM approach. Deshmukh et al. (2004) also used phase analysis to determine clusters of functionally connected brain areas. Recently, phase analysis was proposed to be a measure of dynamic FC (Glerean et al. 2012). In addition, other studies have also explored the dynamics of the complex phase of the BOLD signal using wavelet coherence phase (Chang and Glover 2010; Müller et al. 2004). Despite these attempts, phase analysis has not gained popularity in fMRI. One possible reason is that it remains controversial as to what extent the BOLD signal can be considered as multitude of oscillatory waves (Buzsaki and Draguhn 2004; He and Raichle 2009; Zuo et al. 2010) rather than pure fluctuations. In addition, as applying narrowband filtering of data is a necessary requirement when working with instantaneous phases, it remains to be determined which BOLD frequency band best captures functionally relevant information. These issues may thus demotivate one to explore the foundations of possible phase states in BOLD signal.

Nevertheless, we approached the methodological issues of phase analysis in fMRI signals in several ways. First, we visualized the phase traces in 2 frequency bands: 0.0067–0.5 Hz, which is the frequency band after data preprocessing, and 0.01–0.08 Hz, which is commonly used in resting-state fMRI practice (Biswal et al. 1995; Zou et al. 2008; Buckner et al. 2009). Note that in both cases the data are low- and high-pass filtered, resulting in a relatively narrower band (compared with strictly low-pass filtered data), making the Hilbert phase an appropriate tool. By comparing the phase traces from the 2 frequencies, we found that the Hilbert transform seems to capture the dominant instantaneous phases of the signal in 0.0067–0.5 Hz, which looks similar to the phase traces of 0.01–0.08 Hz albeit more fluctuating. This indicates that the phase traces from the 2 frequencies may share similar functionally relevant information (Fig. 6A). Second, we replicated the whole-brain FC matrices/pattern (Pearson correlations) using Hilbert phase and amplitude as well as phase synchronization analysis in both frequency ranges. This serves as a validation of phase analysis on the basis of traditional FC. Third, we confirmed our phase-based interaction analysis during the task in both frequencies, and we observed similar results (see Supplementary Figs 5 and 6; Supplementary Table 5). Finally, we confirmed that comparing trials with prestimulus-trough phase (0.5π to -0.5π) to prestimulus-peak phase (-0.5π to 0.5π) by phase-based analysis yields almost the same results as when comparing prestimulus low and high magnitude by magnitude-based analysis (Supplementary Fig. 4). This suggests that the instantaneous phase values from fMRI signal are not something arbitrary, and that they can at least capture well the "up-and-down states" (He and Raichle 2009). Despite the above validation and confirmation, and given the complex relationships among the fMRI signal, neuronal firing, and local filed potentials, a full understanding of the nature of the phase cycles of fMRI signals underlying the present observations warrants future investigations.

Unlike our task-fMRI session during which the button press was monitored to ensure participant cooperation and alertness, no measures to maintain or monitor participants' wakefulness were applied during our "eyes closed" resting-state fMRI acquisition. Although no subjects reported falling asleep in this session, we remain unable to unequivocally ensure a stable wakefulness in participants, which may potentially affect our resting-sate

measures in characterizing spontaneous dynamic (e.g., Tagliazucchi and Laufs 2014). Future investigations are needed with wakefulness monitoring during scanning, as well as during different levels of wakefulness such as in vegetative state and under anesthesia (Huang et al. 2015). This may in turn allow us to further address how the level of wakefulness impacts the interaction between spontaneous and evoked activity.

Conclusions

To our knowledge, we have provided for the first time direct evidence for a nonadditive interaction between spontaneous and evoked brain activity and a candidate underlying mechanism, phase-dependent excitability, along with its relationship to the temporal structure of the spontaneous activity. Our results suggest that the temporal structure of spontaneous activity (indexed by both power-law exponent and phase–amplitude coupling) shapes the nonadditive phase-dependent interaction between spontaneous and evoked activity. Our findings not only contribute to our understanding of spontaneous brain activity and its scale-free properties, but also bear important implications for future understanding and analyses of neural activity in general.

Supplementary Material

Supplementary material can be found at: http://www.cercor.oxfordjournals.org/.

Funding

This work was supported by the National Science Foundation of China (No. 31371134 to X.W.; No. 3147107 to N.W.D.), the National Social Science Foundation of China (No. 11AZD119 to X.W.), the EJLB-Michael Smith Foundation, the Canada Institute of Health Research (CIHR), and the Hope of Depression Foundation (HDRF) (to G.N.).

Notes

We thank Dr Biyu He for helpful discussions and two anonymous reviewers for constructive comments. *Conflict of Interest*: None declared.

References

Arieli A, Sterkin A, Grinvald A, Aertsen A. 1996. Dynamics of ongoing activity: explanation of the large variability in evoked cortical responses. Science. 273:1868–1871.

Azouz R, Gray CM. 1999. Cellular mechanisms contributing to response variability of cortical neurons in vivo. J Neurosci. 19:2209–2223.

Becker R, Reinacher M, Freyer F, Villringer A, Ritter P. 2011. How ongoing neuronal oscillations account for evoked fMRI variability. J Neurosci. 31:11016–11027.

Berkes P, Orbán G, Lengyel M, Fiser J. 2011. Spontaneous cortical activity reveals hallmarks of an optimal internal model of the environment. Science. 331:83–87.

Biswal B, Zerrin Yetkin F, Haughton VM, Hyde JS. 1995. Functional connectivity in the motor cortex of resting human brain using echo-planar mri. Magn Reson Med. 34:537–541.

Boly M, Balteau E, Schnakers C, Degueldre C, Moonen G, Luxen A, Phillips C, Peigneux P, Maquet P, Laureys S. 2007. Baseline brain activity fluctuations predict somatosensory perception in humans. Proc Natl Acad Sci USA. 104:12187–12192.

Boynton GM, Engel SA, Glover GH, Heeger DJ. 1996. Linear systems analysis of functional magnetic resonance imaging in human V1. J Neurosci. 16:4207–4221.

Buckner RL, Sepulcre J, Talukdar T, Krienen FM, Liu H, Hedden T, Andrews-Hanna JR, Sperling R, Johnson K. 2009. Cortical hubs revealed by intrinsic functional connectivity: mapping, assessment of stability, and relation to Alzheimer's disease. J Neurosci. 29:1860–1873.

Bullmore E, Long C, Suckling J, Fadiwj J, Calvertl G, Zelaya F, Carpenter TA, Brammers M. 2001. Colored noise and computational inference in fMRI time series analysis : resampling methods in time and wavelet domains. Hum Brain Mapp. 12:61–78.

Buonomano DV, Maass W. 2009. State-dependent computations: spatiotemporal processing in cortical networks. Nat Rev Neurosci. 10:113–125.

Buzsaki G, Draguhn A. 2004. Neuronal oscillations in cortical networks. Science. 304:1926–1929.

Canolty RT, Edwards E, Dalal SS, Soltani M, Nagarajan SS, Kirsch HE, Berger MS, Barbaro NM, Knight RT. 2006. High gamma power is phase-locked to theta oscillations in human neocortex. Science. 313:1626–1628.

Carandini M. 2004. Amplification of Trial-to-Trial Response Variability by Neurons in Visual Cortex. PLoS Biol. 2:e264.

Chai XJ, Castañán AN, Öngür D, Whitfield-Gabrieli S. 2012. Anticorrelations in resting state networks without global signal regression. Neuroimage. 59:1420–1428.

Chang C, Glover GH. 2010. Time-frequency dynamics of resting-state brain connectivity measured with fMRI. Neuroimage. 50:81–98.

Chang MH, Armstrong KM, Moore T. 2012. Dissociation of response variability from firing rate effects in frontal eye field neurons during visual stimulation, working memory, and attention. J Neurosci. 32:2204–2216.

Chialvo DR. 2010. Emergent complex neural dynamics. Nat Phys. 6:744–750.

Churchland MM, Yu BM, Cunningham JP, Sugrue LP, Cohen MR, Corrado GS, Newsome WT, Clark AM, Hosseini P, Scott BB, et al. 2010. Stimulus onset quenches neural variability: a widespread cortical phenomenon. Nat Neurosci. 13:369–378.

Cole MW, Bassett DS, Power JD, Braver TS, Petersen SE. 2014. Intrinsic and task-evoked network architectures of the human brain. Neuron. 83:238–251.

Dechent P, Schütze G, Helms G, Merboldt KD, Frahm J. 2011. Basal cerebral blood volume during the poststimulation undershoot in BOLD MRI of the human brain. J Cereb Blood Flow Metab. 31:82–89.

Deshmukh AV, Shivhare V, Gadre VM, Patkar DP, Pungavkar S. 2004. A phase based method for investigating the functional connectivity in the fMRI data. Proc IEEE INDICON 272–277. doi:10.1109/INDICO.2004.1497754.

Eickhoff SB, Stephan KE, Mohlberg H, Grefkes C, Fink GR, Amunts K, Zilles K. 2005. A new SPM toolbox for combining probabilistic cytoarchitectonic maps and functional imaging data. Neuroimage. 25:1325–1335.

Finn IM, Priebe NJ, Ferster D. 2007. The emergence of contrast-invariant orientation tuning in simple cells of cat visual cortex. Neuron. 54:137–152.

Fox MD, Raichle ME. 2007. Spontaneous fluctuations in brain activity observed with functional magnetic resonance imaging. Nat Rev Neurosci. 8:700–711.

Fox MD, Snyder AZ, Vincent JL, Corbetta M, Van Essen DC, Raichle ME. 2005. The human brain is intrinsically organized into dynamic, anticorrelated functional networks. Proc Natl Acad Sci USA. 102:9673–9678.

Fox MD, Snyder AZ, Zacks JM, Raichle ME. 2006. Coherent spontaneous activity accounts for trial-to-trial variability in human evoked brain responses. Nat Neurosci. 9:23–25.

Fransson P, Metsäranta M, Blennow M, Åden U, Lagercrantz H, Vanhatalo S. 2013. Early development of spatial patterns of power-law frequency scaling in fMRI resting-state and EEG data in the newborn brain. Cereb Cortex. 23:638–646.

Garcia-perez E, Mazzoni A, Torre V. 2007. Hirudo medicinalis. Front Integr Neurosci. 1:1–9.

Glerean E, Salmi J, Lahnakoski JM, Jääskeläinen IP, Sams M. 2012. Functional magnetic resonance imaging phase synchronization as a measure of dynamic functional connectivity. Brain Connect. 2:91–101.

Glover GH, Li TQ, Ress D. 2000. Image-based method for retrospective correction of physiological motion effects in fMRI: RETROICOR. Magn Reson Med. 44:162–167.

Goebel R, Van Atteveldt N. 2009. Multisensory functional magnetic resonance imaging: A future perspective. Exp Brain Res. 198:153–164.

Gonzalez-Castillo J, Saad ZS, Handwerker DA, Inati SJ, Brenowitz N, Bandettini PA. 2012. Whole-brain, time-locked activation with simple tasks revealed using massive averaging and model-free analysis. Proc Natl Acad Sci USA. 109:5487–5492.

Haller S, Wetzel SG, Radue EW, Bilecen D. 2006. Mapping continuous neuronal activation without an ON-OFF paradigm: Initial results of BOLD ceiling fMRI. Eur J Neurosci. 24: 2672–2678.

Haslinger R, Ulbert I, Moore CI, Brown EN, Devor A. 2006. Analysis of LFP phase predicts sensory response of barrel cortex. J Neurophysiol. 96:1658–1663.

He BJ. 2014. Scale-free brain activity: past, present, and future. Trends Cogn Sci. 18:480–487.

He BJ. 2011. Scale-free properties of the functional magnetic resonance imaging signal during rest and task. J Neurosci. 31:13786–13795.

He BJ. 2013. Spontaneous and task-evoked brain activity negatively interact. J Neurosci. 33:4672–4682.

He BJ, Raichle ME. 2009. The fMRI signal, slow cortical potential and consciousness. Trends Cogn Sci. 13:302–309.

He BJ, Snyder AZ, Vincent JL, Epstein A, Shulman GL, Corbetta M. 2007. Breakdown of Functional Connectivity in Frontoparietal Networks Underlies Behavioral Deficits in Spatial Neglect. Neuron. 53:905–918.

He BJ, Zempel JM. 2013. Average Is Optimal: An Inverted-U Relationship between Trial-to-Trial Brain Activity and Behavioral Performance. PLoS Comput Biol. 9:e1003348.

He BJ, Zempel JM, Snyder AZ, Raichle ME. 2010. The temporal structures and functional significance of scale-free brain activity. Neuron. 66:353–369.

Hesselmann G, Kell CA, Eger E, Kleinschmidt A. 2008. Spontaneous local variations in ongoing neural activity bias perceptual decisions. Proc Natl Acad Sci USA. 105:10984–10989.

Hesselmann G, Kell CA, Kleinschmidt A. 2008. Ongoing activity fluctuations in hMT+ bias the perception of coherent visual motion. J Neurosci. 28:14481–14485.

Hua J, Stevens RD, Huang AJ, Pekar JJ, van Zijl PC. 2011. Physiological origin for the BOLD poststimulus undershoot in human brain: vascular compliance versus oxygen metabolism. J Cereb Blood Flow Metab. 31:1599–1611.

Huang Z, Dai R, Wu X, Yang Z, Liu D, Hu J, Gao L, Tang W, Mao Y, Jin Y, et al. 2014. The self and its resting state in consciousness: An investigation of the vegetative state. Hum Brain Mapp. 35:1997–2008.

Huang Z, Wang Z, Zhang J, Dai R, Wu J, Li Y, Liang W, Mao Y, Yang Z, Holland G, et al. 2014. Altered temporal variance and neural synchronization of spontaneous brain activity in anesthesia. Hum Brain Mapp. 5378:5368–5378.

Huang Z, Zhang J, Wu J, Qin P, Wu X, Wang Z, Dai R, Li Y, Liang W, Mao Y, et al. 2015. Decoupled temporal variability and signal synchronization of spontaneous brain activity in loss of consciousness: An fMRI study in anesthesia. Neuroimage. doi: 10.1016/j.neuroimage.2015.08.062.

Johnstone T, Ores Walsh KS, Greischar LL, Alexander AL, Fox AS, Davidson RJ, Oakes TR. 2006. Motion correction and the use of motion covariates in multiple-subject fMRI analysis. Hum Brain Mapp. 27:779–788.

Lachaux JP, Rodriguez E, Martinerie J, Varela FJ. 1999. Measuring phase synchrony in brain signals. Hum Brain Mapp. 8:194–208.

Laird AR, Rogers BP, Carew JD, Arfanakis K, Moritz CH, Meyerand ME. 2002. Characterizing instantaneous phase relationships in whole-brain fMRI activation data. Hum Brain Mapp. 16:71–80.

Lakatos P, Karmos G, Mehta AD, Ulbert I, Schroeder CE. 2008. Entrainment of neuronal oscillations as a mechanism of attentional selection. Science. 320:110–113.

Le Van Quyen M, Bragin A. 2007. Analysis of dynamic brain oscillations: methodological advances. Trends Neurosci. 30:365–373.

Le Van Quyen M, Foucher J, Lachaux J, Rodriguez E, Lutz A, Martinerie J, Varela FJ. 2001. Comparison of Hilbert transform and wavelet methods for the analysis of neuronal synchrony. J Neurosci Methods. 111:83–98.

Linkenkaer-Hansen K, Nikouline VV, Palva JM, Ilmoniemi RJ. 2001. Long-range temporal correlations and scaling behavior in human brain oscillations. J Neurosci. 21:1370–1377.

Logothetis NK, Pauls J, Augath M, Trinath T, Oeltermann A. 2001. Neurophysiological investigation of the basis of the fMRI signal. Nature. 412:150–157.

Lowen SB, Cash SS, Poo M, Teich MC. 1997. Quantal neurotransmitter secretion rate exhibits fractal behavior. J Neurosci. 17:5666–5677.

Lowen SB, Ozaki T, Kaplan E, Saleh BE, Teich MC. 2001. Fractal features of dark, maintained, and driven neural discharges in the cat visual system. Methods. 24:377–394.

Luczak A, Barthó P, Harris KD. 2009. Spontaneous events outline the realm of possible sensory responses in neocortical populations. Neuron. 62:413–425.

Manning JR, Jacobs J, Fried I, Kahana MJ. 2009. Broadband shifts in local field potential power spectra are correlated with single-neuron spiking in humans. J Neurosci. 29: 13613–13620.

Marcos E, Pani P, Brunamonti E, Deco G, Ferraina S, Verschure P. 2013. Neural variability in premotor cortex is modulated by trial history and predicts behavioral performance. Neuron. 78:249–255.

Mayhew SD, Hylands-White N, Porcaro C, Derbyshire SWG, Bagshaw AP. 2013. Intrinsic variability in the human response to pain is assembled from multiple, dynamic brain processes. Neuroimage. 75:68–78.

Miller KJ, Sorensen LB, Ojemann JG, Den Nijs M. 2009. Power-law scaling in the brain surface electric potential. PLoS Comput Biol. 5:e1000609.

Monto S, Palva S, Voipio J, Palva JM. 2008. Very slow EEG fluctuations predict the dynamics of stimulus detection and oscillation amplitudes in humans. J Neurosci. 28:8268–8272.

Morosan P, Rademacher J, Schleicher A, Amunts K, Schormann T, Zilles K. 2001. Human primary auditory cortex: cytoarchitectonic

subdivisions and mapping into a spatial reference system. Neuroimage. 13:684–701.
Müller K, Lohmann G, Neumann J, Grigutsch M, Mildner T, von Cramon DY. 2004. Investigating the wavelet coherence phase of the BOLD signal. J Magn Reson Imaging. 20:145–152.
Nir Y, Fisch L, Mukamel R, Gelbard-Sagiv H, Arieli A, Fried I, Malach R. 2007. Coupling between Neuronal Firing Rate, Gamma LFP, and BOLD fMRI Is Related to Interneuronal Correlations. Curr Biol. 17:1275–1285.
Northoff G, Qin P, Nakao T. 2010. Rest-stimulus interaction in the brain: A review. Trends Neurosci. 33:277–284.
Palva JM, Palva S. 2012. Infra-slow fluctuations in electrophysiological recordings, blood-oxygenation-level-dependent signals, and psychophysical time series. Neuroimage. 62:2201–2211.
Palva JM, Zhigalov A, Hirvonen J, Korhonen O, Linkenkaer-Hansen K, Palva S. 2013. Neuronal long-range temporal correlations and avalanche dynamics are correlated with behavioral scaling laws. Proc Natl Acad Sci USA. 110:3585–3590.
Poline JB, Brett M. 2012. The general linear model and fMRI: Does love last forever? Neuroimage. 62:871–880.
Power JD, Cohen AL, Nelson SM, Wig GS, Barnes KA, Church JA, Vogel AC, Laumann TO, Miezin FM, Schlaggar BL, et al. 2011. Functional network organization of the human brain. Neuron. 72:665–678.
Raichle ME, Mintun MA. 2006. Brain work and brain imaging. Annu Rev Neurosci. 29:449–476.
Rubin D, Fekete T, Mujica-Parodi LR. 2013. Optimizing Complexity Measures for fMRI Data: Algorithm, Artifact, and Sensitivity. PLoS One. 8:e63448.
Saad ZS, DeYoe EA, Ropella KM. 2003. Estimation of FMRI response delays. Neuroimage. 18:494–504.
Sadaghiani S, Hesselmann G, Kleinschmidt A. 2009. Distributed and antagonistic contributions of ongoing activity fluctuations to auditory stimulus detection. J Neurosci. 29:13410–13417.
Sadaghiani S, Scheeringa R, Lehongre K, Morillon B, Giraud A-L, Kleinschmidt A. 2010. Intrinsic connectivity networks, alpha oscillations, and tonic alertness: a simultaneous electroencephalography/functional magnetic resonance imaging study. J Neurosci. 30:10243–10250.
Saka M, Berwick J, Jones M. 2010. Linear superposition of sensory-evoked and ongoing cortical hemodynamics. Front Neuroenergetics. 2:1–13.
Scaglione A, Moxon KA, Aguilar J, Foffani G. 2011. Trial-to-trial variability in the responses of neurons carries information about stimulus location in the rat whisker thalamus. Proc Natl Acad Sci USA. 108:14956–14961.
Scheeringa R, Mazaheri A, Bojak I, Norris DG, Kleinschmidt A. 2011. Modulation of visually evoked cortical FMRI responses by phase of ongoing occipital alpha oscillations. J Neurosci. 31:3813–3820.
Schurger A, Sarigiannidis I, Naccache L, Sitt JD, Dehaene S. 2015. Cortical activity is more stable when sensory stimuli are consciously perceived. Proc Natl Acad Sci USA. 112:E2083–E2092.
Scott SK, Johnsrude IS. 2003. The neuroanatomical and functional organization of speech perception. Trends Neurosci. 26:100–107.
Stephens GJ, Honey CJ, Hasson U. 2013. A place for time: the spatiotemporal structure of neural dynamics during natural audition. J Neurosci. 110:2019–2026.
Sylvester CM, Shulman GL, Jack AI, Corbetta M. 2009. Anticipatory and stimulus-evoked blood oxygenation level-dependent modulations related to spatial attention reflect a common additive signal. J Neurosci. 29:10671–10682.
Tagliazucchi E, Laufs H. 2014. Decoding wakefulness levels from typical fMRI resting-state data reveals reliable drifts between wakefulness and sleep. Neuron. 82:695–708.
Tort ABL, Kramer MA, Thorn C, Gibson DJ, Kubota Y, Graybiel AM, Kopell NJ. 2008. Dynamic cross-frequency couplings of local field potential oscillations in rat striatum and hippocampus during performance of a T-maze task. Proc Natl Acad Sci USA. 105:20517–20522.
Vanhatalo S, Palva JM, Holmes MD, Miller JW, Voipio J, Kaila K. 2004. Infraslow oscillations modulate excitability and interictal epileptic activity in the human cortex during sleep. Proc Natl Acad Sci USA. 101:5053–5057.
White B, Abbott LF, Fiser J. 2012. Suppression of cortical neural variability is stimulus- and state-dependent. J Neurophysiol. 108:2383–2392.
Yacoub E, Ugurbil K, Harel N. 2006. The spatial dependence of the poststimulus undershoot as revealed by high-resolution BOLD- and CBV-weighted fMRI. J Cereb Blood Flow Metab. 26:634–644.
Yang H, Shew WL, Roy R, Plenz D. 2012. Maximal variability of phase synchrony in cortical networks with neuronal avalanches. J Neurosci. 32:1061–1072.
Zou QH, Zhu CZ, Yang Y, Zuo XN, Long XY, Cao QJ, Wang YF, Zang YF. 2008. An improved approach to detection of amplitude of low-frequency fluctuation (ALFF) for resting-state fMRI: Fractional ALFF. J Neurosci Methods. 172:137–141.
Zuo XN, Di Martino A, Kelly C, Shehzad ZE, Gee DG, Klein DF, Castellanos FX, Biswal BB, Milham MP. 2010. The oscillating brain: Complex and reliable. Neuroimage. 49:1432–1445.